



Fiber lattice accumulator design considerations for optical [sigma-delta] digital antennas

Title	Fiber lattice accumulator design considerations for optical [sigma-delta] digital antennas
Item Type	Thesis
Authors	Bewley, Scott A.
URI	https://hdl.handle.net/10945/8404
Publisher	Monterey, California. Naval Postgraduate School
Date Issued	1998-12-01
Rights	This publication is a work of the U.S. Government as defined in Title 17, United States Code, Section 101. Copyright protection is not available for this work in the United States.
Download date	2026-04-14 05:49:13
Link to Item	https://hdl.handle.net/10945/8404

Downloaded from NPS Archive: Calhoun

NPS ARCHIVE
1998.12
BEWLEY, S.

DUDLEY KNOX LIBRARY
NAVAL POSTGRADUATE SCHOOL
MONTEREY, CA 93943-5101

DUDLEY KNOX LIBRARY
NAVAL POSTGRADUATE SCHOOL
MONTEREY CA 93943-5101

NAVAL POSTGRADUATE SCHOOL

Monterey, California



THESIS

**FIBER LATTICE ACCUMULATOR DESIGN
CONSIDERATIONS FOR OPTICAL $\Sigma\Delta$ DIGITAL
ANTENNAS**

by

Scott A. Bewley

December 1998

Thesis Advisor:
Co-Advisor:

Phillip E. Pace
James H. Luscombe

Approved for public release; distribution is unlimited.

REPORT DOCUMENTATION PAGE

Form Approved OMB No. 0704-0188

Public reporting burden for this collection of information is estimated to average 1 hour per response, including the time for reviewing instruction, searching existing data sources, gathering and maintaining the data needed, and completing and reviewing the collection of information. Send comments regarding this burden estimate or any other aspect of this collection of information, including suggestions for reducing this burden, to Washington headquarters Services, Directorate for Information Operations and Reports, 1215 Jefferson Davis Highway, Suite 1204, Arlington, VA 22202-4302, and to the Office of Management and Budget, Paperwork Reduction Project (0704-0188) Washington DC 20503.

1. AGENCY USE ONLY (Leave blank)		2. REPORT DATE December 1998	3. REPORT TYPE AND DATES COVERED Master's Thesis	
4. TITLE AND SUBTITLE Fiber Lattice Accumulator Design Considerations for Optical $\Sigma\Delta$ Digital Antennas			5. FUNDING NUMBERS	
6. AUTHOR(S) Bewley, Scott A.			8. PERFORMING ORGANIZATION REPORT NUMBER	
7. PERFORMING ORGANIZATION NAME(S) AND ADDRESS(ES) Naval Postgraduate School Monterey, CA 93943-5000			10. SPONSORING/MONITORING AGENCY REPORT NUMBER	
9. SPONSORING / MONITORING AGENCY NAME(S) AND ADDRESS(ES) Center for Reconnaissance			11. SUPPLEMENTARY NOTES The views expressed in this thesis are those of the author and do not reflect the official policy or position of the Department of Defense or the U.S. Government.	
12a. DISTRIBUTION / AVAILABILITY STATEMENT Approved for public release; distribution is unlimited.			12b. DISTRIBUTION CODE	
13. ABSTRACT (maximum 200 words) <p>The ability to directly oversample and digitize microwave range signals at an antenna is not possible with current electronic technologies. The objective for this thesis was to design and computer model an optical sampling and digitization process using a mode-locked laser and fiber lattice accumulators. A novel fiber lattice accumulator design for integrated optical sigma-delta ($\Sigma\Delta$) digital antenna technology is presented. The fiber lattice design uses phase modulation to produce the proper interference between input and recirculated/delayed optical pulses in order that they may coherently combine. In this manner, accumulation within the fiber lattice takes into account the sign of a sampled bipolar antenna signal. The fiber lattice performance is numerically evaluated within a first-order optical $\Sigma\Delta$ digital antenna phase coherent simulation. The initial computer simulations show promising results using lower frequency antenna signals to verify optical design feasibility and operation. Optical results closely matched all-electronic simulations. The error between the input antenna and output signals is quantified, and proves correct device performance. All results show the first-order optical $\Sigma\Delta$ does work and is ready for experimental construction. The significance of this device will be its usefulness in extending high resolution $\Sigma\Delta$ analog-to-digital conversion into the microwave signal bands.</p>				
14. SUBJECT TERMS ADC, Fiber Lattice Structures, Sigma-Delta, Directional Coupler, Oversampling, Optical ADC, Phase Coherent Modeling			15. NUMBER OF PAGES 70	
			16. PRICE CODE	
17. SECURITY CLASSIFICATION OF REPORT Unclassified	18. SECURITY CLASSIFICATION OF THIS PAGE Unclassified	19. SECURITY CLASSIFICATION OF ABSTRACT Unclassified	20. LIMITATION OF ABSTRACT UL	

Approved for public release; distribution is unlimited

**FIBER LATTICE ACCUMULATOR DESIGN CONSIDERATIONS FOR
OPTICAL $\Sigma\Delta$ DIGITAL ANTENNAS**

Scott A. Bewley
Lieutenant, United States Navy
B.S., North Carolina State University, 1991

Submitted in partial fulfillment of the
requirements for the degree of

MASTER OF SCIENCE IN APPLIED PHYSICS

from the

**NAVAL POSTGRADUATE SCHOOL
December 1998**

n

ABSTRACT

The ability to directly oversample and digitize microwave range signals at an antenna is not possible with current electronic technologies. The objective for this thesis was to design and computer model an optical sampling and digitization process using a mode-locked laser and fiber lattice accumulators. A novel fiber lattice accumulator design for integrated optical sigma-delta ($\Sigma\Delta$) digital antenna technology is presented. The fiber lattice design uses phase modulation to produce the proper interference between input and recirculated/delayed optical pulses in order that they may coherently combine. In this manner, accumulation within the fiber lattice takes into account the sign of a sampled bipolar antenna signal. The fiber lattice performance is numerically evaluated within a first-order optical $\Sigma\Delta$ digital antenna phase coherent simulation. The initial computer simulations show promising results using lower frequency antenna signals to verify optical design feasibility and operation. Optical results closely matched all-electronic simulations. The error between the input antenna and output signals is quantified, and proves correct device performance. All results show the first-order optical $\Sigma\Delta$ does work and is ready for experimental construction. The significance of this device will be its usefulness in extending high resolution $\Sigma\Delta$ analog-to-digital conversion into the microwave signal bands.

TABLE OF CONTENTS

I.	INTRODUCTION	1
	A. BACKGROUND	1
	B. PRINCIPLE CONTRIBUTIONS	2
	C. THESIS OUTLINE	3
II.	OVERSAMPLING ALL-ELECTRONIC SIGMA-DELTA ($\Sigma\Delta$) ANALOG-TO-DIGITAL (A/D) CONVERTER	5
	A. INTRODUCTION	5
	B. OVERSAMPLING $\Sigma\Delta$ ADC THEORY AND DESCRIPTION	5
	1. Oversampling Theory	5
	2. Sigma-Delta ($\Sigma\Delta$) Modulation	7
	3. Single-Bit All-Electronic Oversampling $\Sigma\Delta$ ADCs	8
	4. Decimation Filtering	11
	C. MODELING THE ALL-ELECTRONIC $\Sigma\Delta$ ADC	11
	1. Accumulator Design and Modeling Considerations	12
	2. Output Comparator	13
	3. Oversampling Simulations	13
	4. Decimation Filter Model	14
	D. RESULTS AND CONCLUSIONS	15
III.	INTEGRATED OPTICAL $\Sigma\Delta$ DIGITAL ANTENNAS	19
	A. OVERVIEW	19
	B. OPTICAL $\Sigma\Delta$ DIGITAL ANTENNAS	20
	C. OPTICAL COMPONENTS AND PHASE COHERENT MODELING	21
	1. Mode-Locked Laser	21
	<i>a. Theory and Description</i>	21
	<i>b. Phase Coherent Model</i>	22
	2. Mach-Zehnder Interferometers	23
	<i>a. Theory and Description</i>	23
	<i>b. Phase Coherent Model</i>	25
	3. Fiber Lattice Structure	27
	<i>a. Theory and Description</i>	27
	<i>b. Directional Coupler Models</i>	29
	<i>c. Phase Coherent Model</i>	31
	4. Output Photodetector	33
	5. Output Comparator	34
	6. Decimation Filtering	34
	D. RESULTS FOR FIRST-ORDER DESIGNS	34
	E. CONCLUSIONS	37
IV.	LIMITATIONS, CONCLUSIONS, AND RECOMMENDATIONS	39
	A. LIMITATIONS	39
	B. CONCLUSIONS	39
	C. RECOMMENDATIONS	40

APPENDIX A. ALL-ELECTRONIC $\Sigma\Delta$ SIMULINK PROGRAM MODELS	41
APPENDIX B. OPTICAL $\Sigma\Delta$ SIMULINK PROGRAM MODEL	45
APPENDIX C. PROGRAMS FOR COMPARISON OF ALL-ELECTRONIC AND OPTICAL ACCUMULATORS.....	49
APPENDIX D. PHASE COHERENT SECOND-ORDER OPTICAL $\Sigma\Delta$ DIGITAL ANTENNA	51
APPENDIX E. MACH-ZEHNDER INTERFEROMETER MAGNITUDE AND DIRECTION PROGRAMS	53
APPENDIX F. PHASE COHERENT SIMULINK PROGRAMS FOR MACH-ZEHNDER INTERFEROMETERS	55
LIST OF REFERENCES.....	57
INITIAL DISTRIBUTION LIST	59

ACKNOWLEDGEMENT

First and foremost, I would like to thank those who helped me achieve this invaluable goal. One in particular was Professor Pace, whose positive attitude and endless capacity for new ideas pushed me through my darkest hour to achieve success on this thesis. Another was Professor Jovan LeBaric, whose help was priceless in solving the detector problem which plagued me for weeks.

I would like to dedicate this thesis to my wife who has stood by me with encouragement and patience. She is the center of my life and without her unconditional love and support, I don't think it would have been nearly as nice an experience. I look forward to overcoming many more challenges and milestones with her by my side.

Also to my good friends and shipmates, Pierre Hilaire, John Holmes, Ty Britt, and Mustafa Yvanc for helping me find new levels of learning and friendship, within our study groups and on the golf course (farewell Bayonet and Blackhorse, I shall be victorious some day).

This work was supported by the Naval Postgraduate School Center for Reconnaissance.

I. INTRODUCTION

A. BACKGROUND

Analog-to-digital converters (ADCs) are extremely important components in the modern world of electronic systems. They provide the critical translation of the measured analog signals into the digital realm so that filtering, modification, analysis, and processing can be performed. A partial list of some ADC applications includes process control, automatic test equipment, video signal acquisition, audio recordings for compact discs, and interfaces for personal computers. Unfortunately, the process of converting an analog signal is limited by the speed and resolution capability of the sampling and filtering device. As a result, a great deal of research has been conducted on high speed, high resolution ADCs. One device that has found widespread popularity for improving signal resolution is the oversampling sigma-delta ($\Sigma\Delta$) ADC filter architecture.

The primary advantages of the oversampling $\Sigma\Delta$ ADC is its increased resolution capability without the use of complicated circuitry. It is also simple to integrate into most systems due to analog signal processing component requirements that are much less than the overall resolution capability of the converter. In its most basic form, it only requires a 1-bit ADC.

Oversampling $\Sigma\Delta$ analog-to-digital (A/D) conversion is the combination of two processes acting together. The first is the oversampling of the analog signal. This is a technique for sampling higher than the Nyquist rate to improve resolution. Sigma-Delta Modulation ($\Sigma\Delta M$) is a noise shaping filter which can further improve resolution when applied to an oversampled signal. It uses integration and feedback in iterative loops to

track the incoming oversampled signal, and calculate and subtract off the quantization error.

Oversampling $\Sigma\Delta$ A/D conversion is a well documented technique which has found applications in many areas. Some of these include audio, telecommunications, medical imaging, and cellular phones. One drawback, which has limited its bandwidth application in the past, is the inability to obtain oversampling rates sufficient to sample signals in the higher frequency bandwidths. To achieve a given precision, the input sample rate of the $\Sigma\Delta$ ADC must be significantly higher than the conversion rate. Because of this, its use has been restricted mostly to lower frequencies and smaller bandwidths due to the sampling rate limitations of electronic technology. This thesis explores new areas of $\Sigma\Delta$ ADC within the optical realm in an attempt to discover new ways of increasing sampling rate in order to extend the bandwidth of the $\Sigma\Delta$ ADC into the microwave region of the rf spectrum.

B. PRINCIPLE CONTRIBUTIONS

All-electronic oversampling $\Sigma\Delta$ ADCs have been extensively studied and documented [Ref. 1,2]. The optical $\Sigma\Delta$, on the other hand, has very few documented research efforts [Ref. 3,4,5,6]. The initial documentation used in this thesis came from previous thesis work performed at the Naval Postgraduate school [Ref. 6, 7].

This thesis is divided into two distinct parts. The first consists of the theory and modeling of the all-electronic $\Sigma\Delta$ ADC. The second part covers the optical $\Sigma\Delta$ digital antenna. Computer simulations were developed to model the electronic and optical $\Sigma\Delta$ architectures. Results from the simulations were then compared to determine the feasibility of developing an optical $\Sigma\Delta$ device. The theory and application of mode-

locked lasers[Ref. 8], phase modulators, directional couplers, [Refs. 9,10] and fiber optic lattice signal processing [Refs. 11, 12] is described and integrated into the optical $\Sigma\Delta$ digital antenna design.

C. THESIS OUTLINE

Chapter II covers the basic all-electronic $\Sigma\Delta$ ADC theory and presents computer models and results to build a foundation for comparison to the optical $\Sigma\Delta$ architecture that has been developed. Emphasis was placed on signal demodulation through the process of decimation. The purpose was to produce outputs that could be readily identified and compared with signals obtained from the optical models. Sinusoidal as well as ramp signals were used to test the models.

In Chapter III the phase coherent optical $\Sigma\Delta$ antenna architecture is presented along with a description of each optical component and it's theory and application. A description of developed computer models, results, and comparison analysis to the all-electronic $\Sigma\Delta$ device is provided.

Finally, Chapter IV will offer conclusions, recommendations, and suggestions for further study within this area.

II. OVERSAMPLING ALL-ELECTRONIC SIGMA-DELTA ($\Sigma\Delta$) ANALOG-TO-DIGITAL CONVERTERS (ADCs)

A. INTRODUCTION

Sigma-Delta ($\Sigma\Delta$) modulators and their application in analog-to-digital (A/D) conversion were first proposed in the 1960's, but due to their requirement for high oversampling rates, did not prove practical until recent improvements in technology. Today, the basic theory and operation of $\Sigma\Delta$ modulators is well documented with hundreds of research papers and results. Widespread application has also developed in many areas of technology including cellular phones and audio systems. This thesis will not attempt to fully analyze the all-electronic $\Sigma\Delta$ ADC, but instead, will review basic theory, describe computer modeled simulations, and show results for comparison to the optical $\Sigma\Delta$ digital antenna. A complete description of the $\Sigma\Delta$ theory and application can be found in [Refs. 1, 2].

B. OVERSAMPLING $\Sigma\Delta$ ADC THEORY AND DESCRIPTION

1. Oversampling Theory

Oversampling is the sampling of an analog signal at a rate higher than the Nyquist criteria, $f_s = 2f_0$, where f_s is the sampling frequency and f_0 is the frequency of the input analog signal to be digitized. Quantization noise is a byproduct of the sampling process and usually the dominant source of error introduced into the signal bandwidth when the signal is digitized. Other types of noise, including thermal and jitter noise, are also present, but usually at lower levels.

When sampling occurs at the Nyquist rate, the quantization noise is at the highest level. As the sampling rate increases, a more precise representation of the analog signal

is created and the quantization noise is reduced. This reduction is observed as a lowering of the signal noise-floor, or increase in the signal-to-noise ratio (SNR) in the frequency spectrum [Ref. 1,2]. During oversampling, the same amount of quantization noise found at the Nyquist rate is physically spread over a larger bandwidth associated with the oversampling frequency (f_s). This forces a larger portion of the quantization error outside the signal band. A filter can now be used to remove the out-of-band frequency components leaving the signal band intact. The result is a signal band with an improved SNR. An example of oversampling is shown graphically in Figure 1.

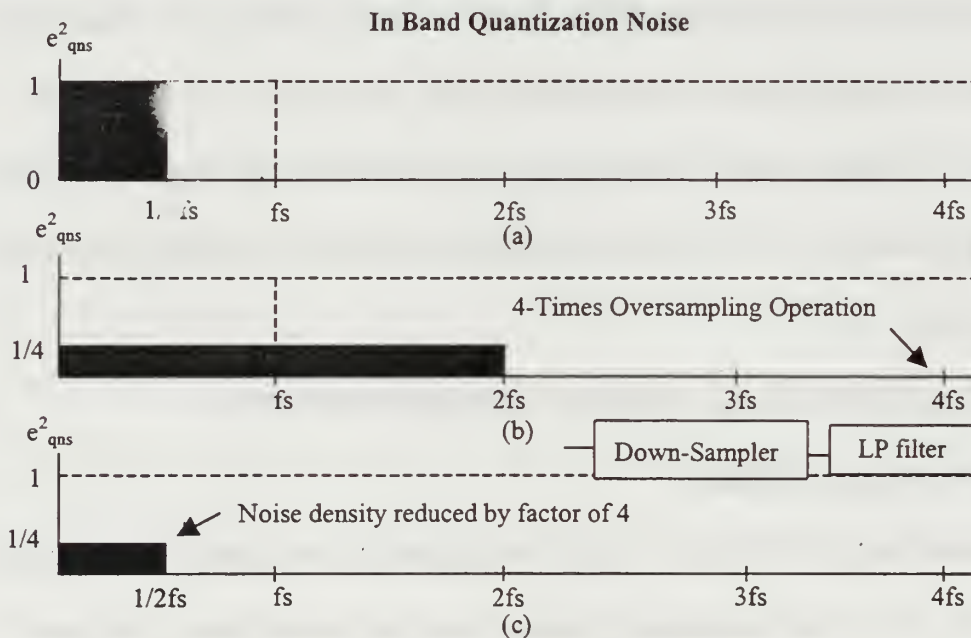


Figure 1: In-band quantization noise power density with (a) Nyquist sampling, (b) oversampling factor of 4, (c) output after filtering.

For calculation and analysis purposes, the amount of oversampling is usually quantified as an oversampling ratio (OSR) that is written

$$OSR = \frac{1}{2f_o\tau_s} = \frac{f_s}{2f_o}. \quad (1)$$

When the OSR doubles, the SNR improves by 3 dB, increasing the resolution of the device by 1.5 bits [Refs. 1, 2].

Oversampling does have limitations. In general, by oversampling a signal, bandwidth is traded for signal resolution. As the sampling rate increases the resolution increases. Concurrently, the bandwidth of the system decreases.

2. Sigma-Delta ($\Sigma\Delta$) Modulation

Sigma-delta ($\Sigma\Delta$) modulation is a noise shaping technique which combines integration and feedback in iterative loops to obtain high resolution A/D conversion. The integration consists of accumulating the quantization error between the sampled input and the feedback signal. When the accumulated error reaches a specific threshold voltage, the output signal is quantized, fed-back, and subtracted from the input. This effectively moves the noise component of the signal up in frequency and outside the signal band. A filter is then used to remove the out-of-band frequency components as in the oversampling technique discussed in Section B1.

The integrator consists of a sample delay ($1/f_s$), a feed back loop which accumulates the signal, and two gain amplifiers which control accumulation rate. Depending on circuit order and architecture, the integrator is modified so the sample delay is either in the feed-forward or feedback path. The reasons and uses for the different integrators will become apparent when the entire $\Sigma\Delta$ A/D converter is introduced in Section B3. Equations 2 and 3 are the transfer functions for the two separate integrator architectures [Ref. 6]

$$H_{FB}(z) = \frac{A}{1 - Bz^{-1}} \quad (2)$$

$$H_{FF}(z) = \frac{Cz^{-1}}{1 - Dz^{-1}} \quad (3)$$

where $H_{FB}(z)$ (Eqn. 2) is the integrator with the delay function in the feedback path and $H_{FF}(z)$ (Eqn. 3) is the integrator with the delay in the feed-forward path. Figure 2 shows both integrator block diagrams. Both work in the same manner with their accumulation

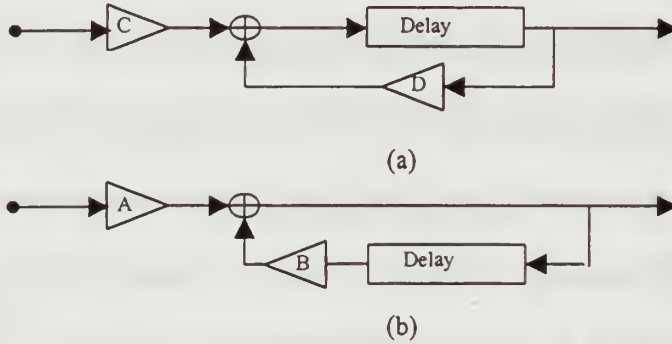


Figure 2: Block Diagrams for $\Sigma\Delta$ Modulator Integrators with the delay Function in the (a) Feed Forward Position ($H_{FF}(z)$) (b) Feedback Position ($H_{FB}(z)$).

rates being the difference between them. The $H_{FF}(z)$ accumulates faster than the $H_{FB}(z)$. The integrator, because it ‘accumulates’ the signal error, is normally referred to as an *accumulator* when discussing the sampled-data $\Sigma\Delta$ ADC.

3. Single-Bit All-Electronic Oversampling $\Sigma\Delta$ ADCs

The oversampling all-electronic $\Sigma\Delta$ ADC uses oversampling, accumulation and decimation (lowpass filtering and re-sampling at the Nyquist rate) to reduce the noise within the signal band. It is essentially a sampled data circuit, and thus, the integration is performed via accumulation [Ref. 6]. The analog signal is assumed oversampled well above the Nyquist frequency. The sampled data is then amplitude analyzed in a comparator/quantizer, which is then fed-back and subtracted from the input. This

quantized feedback signal forces the average value of the quantized output to track the oversampled input signal. Any difference between the two accumulates in the integrator, eventually correcting for the input quantization error [Ref. 6].

By continually calculating and subtracting the quantization error from the oversampled input signal, an accurate, time delayed, digital representation of the input is created that contains a significant SNR improvement over a regularly oversampled signal. The SNR improvement, as with oversampling, is incrementally quantified with the OSR.

For every doubling of the OSR the noise improves $3(2L-1)$ decibels (dBs), providing $L + 1/2$ extra bits of resolution. L is the order of the $\Sigma\Delta$ ADC and is determined by the number of accumulators and feedback loops. A block diagram of a first order $\Sigma\Delta$ ADC is shown in Figure 3a.

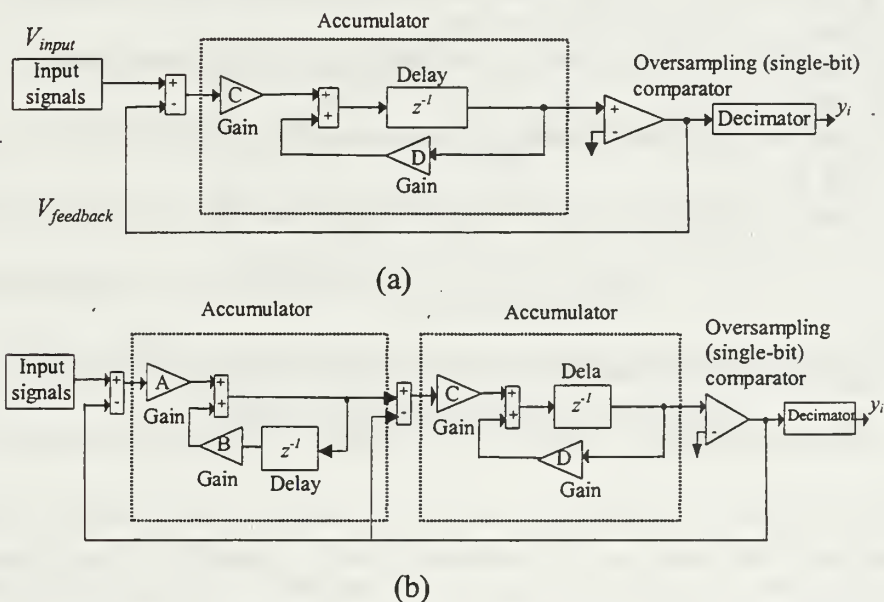


Figure 3: Block diagrams of a (a) 1st order and a (b) 2nd order all-electronic $\Sigma\Delta$ ADC.

The first order single-bit $\Sigma\Delta$ ADC is characterized by a single feedback loop and one accumulator. The accumulator is the integrator $H_{FF}(z)$ (Eqn. 3). The second order,

shown in Figure 3b has two feedback loops and two accumulators. The first accumulator is the integrator $H_{FB}(z)$ (Eqn. 2), whereas, the second accumulator is the $H_{FF}(z)$ (Eqn. 3). The slower accumulator is required in the front so the device will maintain a stable monotonic accumulation rate.

Each additional accumulator improves the SNR in accordance with the relation $3(2L-1)$ dBs. For example, a second order $\Sigma\Delta$ ADC has order $L = 2$ and therefore, 9 dBs or 2.5 extra bits of resolution occur for every doubling of the OSR. As shown in Figure 4 [Ref. 2], it can be determined theoretically that as the order of the device increases the

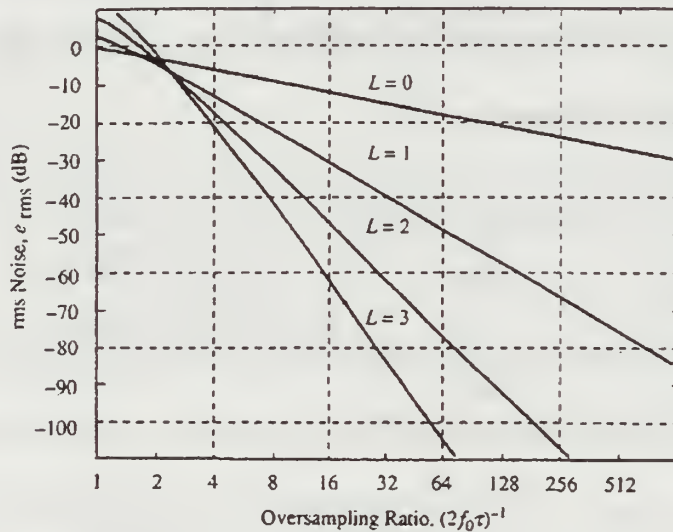


Figure 4: RMS noise that enters the signal band as a function of the oversampling ratio (OSR).

SNR and signal resolution improve. For example, a device of order $L=4$ should produce 21 dBs or 3.5 extra bits of resolution for every doubling of the OSR. On the other hand, higher order $\Sigma\Delta$ architectures tend to be unstable and difficult to model and design. For this reason, first- and second-order $\Sigma\Delta$ s were studied exclusively in this thesis.

4. Decimation Filtering

The output of the $\Sigma\Delta$ modulator consists of the high frequency modulation, out-of-band noise components, and other circuit related noise which dominate at the lower frequencies [Ref. 1]. A decimation filter is used to remove all the quantization/modulation noise and extract the digitized signal. It consists of a lowpass filter and a resampling mechanism to down-sample the signal to the Nyquist rate. This is best accomplished in multiple stages of filtering and resampling. The first stage removes the modulation noise and down-samples the signal to some intermediate sampling frequency. A second lowpass filter is then used to attenuate the out-of-band components before the signal is again resampled at the Nyquist rate. As the signal propagates through the filters and resampling stages, the word length increases to preserve the resolution [Ref. 6]. A more thorough description is found in [Refs. 1, 2].

The decimation filter is not restricted to lowpass filters. Other types of filters can also be used [Ref. 2]. For example, there are passband and stopband decimation filters. For the purpose of this thesis, only lowpass filters were considered.

C. MODELING THE ALL-ELECTRONIC $\Sigma\Delta$ ADC

MATLAB and SIMULINK software was used to model the first- and second-order all-electronic $\Sigma\Delta$ ADCs. The SIMULINK block diagrams are similar to the block diagram in Figure 3 and are shown in Appendix A, Figure A1. Each model consists of the input antenna signal, the feedback loop, the accumulator, and decimator for demodulation.

1. Accumulator Design and Modeling Considerations

In the first-order $\Sigma\Delta$ computer program design (Appendix A, Fig. A1a), the accumulator is modeled by a sample delay ($1/f_s$) function block, a feedback loop with a summation block adding the accumulator feedback into the input signal, and two gain amplifiers blocks. This arrangement simulates the $H_{FF}(z)$ integrator transfer function (Eqn. 3). The gain coefficients, C and D regulate the accumulation rate of the device. Gain values between 0.1 and 1.1 are acceptable for the D gain coefficient. A D gain coefficient higher than 1.1 and the signal will overload the circuit and cause nonlinear accumulation. On the other hand, D coefficients that are too low will not allow sufficient accumulation resulting in signal loss. The C gain coefficient scales the input signal to the desired level. It also effects accumulation rate, but it's effects are not as evident as the dominant D gain coefficient. The best results are achieved when the gain coefficients are all set to 1.0.

In the second-order $\Sigma\Delta$ architecture (Appendix A, Fig A1b), the $H_{FB}(z)$ transfer function (Eqn. 2) is used in the first stage accumulator and the $H_{FF}(z)$ (Eqn. 3) is used in the second stage. The slower accumulator ($H_{FB}(z)$) is used in the first stage to ensure circuit stability. Values for the gain coefficients A , B , C , and D are again between 0.1 and 1.1. Different combinations provide varying accumulation rates and outputs. Both delay function boxes within the accumulators of the second-order are also sample delays ($1/f_s$) as in the first-order. Again, as for the first-order, the best results are achieved when all gain coefficients are set to 1.

2. Output Comparator

The relay function block models a single bit comparator/quantizer, which modulates the signal and the noise, resulting in the noise component being moved up in frequency and outside the signal band. The rate at which the comparator is clocked is the oversampling frequency ($1/f_s$). If the accumulator output voltage exceeds the comparator threshold, $V_T=0$, the comparator output voltage, $V_{feedback} = 1V$. Otherwise, the comparator output voltage, $V_{feedback} = -1V$. The modulated signal ($V_{feedback}$) then feeds back and is subtracted from the oversampled input antenna signal.

The $\Sigma\Delta$ architectures presented in this thesis are single-bit devices and therefore, signal amplitudes greater than ± 1 cannot be accommodated. Multi-level devices are modeled by adding a multi-bit ADC in place of the comparator/quantizer [Ref. 2].

3. Oversampling Simulations

The sampling clock mechanism for oversampling the input signals was performed by computer time steps. The signal was produced using a function block in the SIMULINK program. The number of time steps, representing the signal sampling rate (f_s) were specified depending on the amount of oversampling required. For example, if a 1 Hz signal was modeled and an OSR of 100 was required, then using Equation 1, it can be determined that $f_s=200$ Hz. Then $1/200$ would be entered into the program as the sampling step size. Two types of signals were primarily tested: a ramped signal with a range of $\pm 1V$, and a sine function with an amplitude of $1V$.

4. Decimation Filter Model

The modulated comparator output signal is a combination of the digitized input signal, the modulation noise, and other out-of-band components. A decimation model was developed in SIMULINK to remove the noise and out-of-band components to recover the digitized input signal. The recovered signal was then used for comparison and analysis in the optical $\Sigma\Delta$ design results. Appendix A, Figure A2 shows the SIMULINK computer model designed to demodulate and analyze the recovered signal. It consists of multiple decimation steps, each of which has of a separate lowpass filter and down-sampler. For programming purposes, large down-sampling steps should be avoided due to inaccuracies in the program. This makes the number of decimation filters dependent on the OSR. For example, if the OSR = 100 and the $f_0 = 1$ Hz, then $f_s = 200$ Hz. This requires a down-sample factor of 100 to reduce the sampling rate to $f_{Nyquist} = 2$ Hz, which should be calculated in three decimation steps performed in series. The first two steps each down-sample by a factor of 5 to the intermediate frequency of 8 Hz. The third decimation step then down-samples by a factor of 4 to the Nyquist rate of 2 Hz. A good rule of thumb is: avoid down-sampling factors greater than 8. The lowpass filter design used in the computer models consisted of a 15th order finite impulse response (FIR) lowpass filter with an applied Hamming window for sinusoid signals.

Once decimated the signal is displayed on a scope to view the time-domain. Then the Fast Fourier Transform (FFT) is calculated to view the frequency domain. Appendix A provides the general decimation, FFT, and program parameters to achieve good results.

D. RESULTS AND CONCLUSIONS

The signals of choice for all analysis was a low frequency sine wave usually around 1-4 Hz and a ramp signal with a ± 1 V range. To model high frequency signals on a computer is difficult due to the large amount of computer time steps required to obtain accurate results. Therefore, the frequencies were scaled down to manageable levels to demonstrate the concepts and correct operation of the $\Sigma\Delta$ architecture designs. Figures 5 and 6 show the ramped and sinusoidal antenna input signals and outputs at various stages for the all-electronic first-order $\Sigma\Delta$ design. All-electronic second-order time domain results are very similar to first order and thus are shown in appendix A, Figures A3 and A4. The ramped signal shows a simulation time of 200 samples and a sampling rate of 1 sample per second. The input frequency of the sine signal is $f_0 = 1$ Hz. It's sampling rate is $f_s = 32$ Hz giving an OSR of 16. Figures 5a and 6a are the input input signals and Figures 5b and 6b are the oversampled input signal with the feedback voltage subtracted ($v(t) = V_{input} - V_{feedback}$). Figures 5c and 6c are the output of the $H_{FB}(z)$ accumulator and 5d and 6d are the modulated comparator output ($V_{feedback}$). The final digitized signal can now be filtered from the modulated output via the decimation filter. Figure 7 shows the digitized filtered signal output for both a ramp and sinusoid input. Noise was added to the input signals in Figure 7 to demonstrate how effectively noise is removed in the $\Sigma\Delta$ architecture. The actual output is the smooth signal. The initial step response at the beginning of the ramped output and the phase delay in the sinusoidal output are due to the initial charge-up of the lowpass filter during decimation.

In conclusion, modeling of the all-electronic $\Sigma\Delta$ ADC was successful in providing a baseline of results that could be compared with the optical $\Sigma\Delta$ design presented in Chapter III. The SIMULINK computer models (Appendix A) for the first- and second-order $\Sigma\Delta$ worked as expected and produced good results.

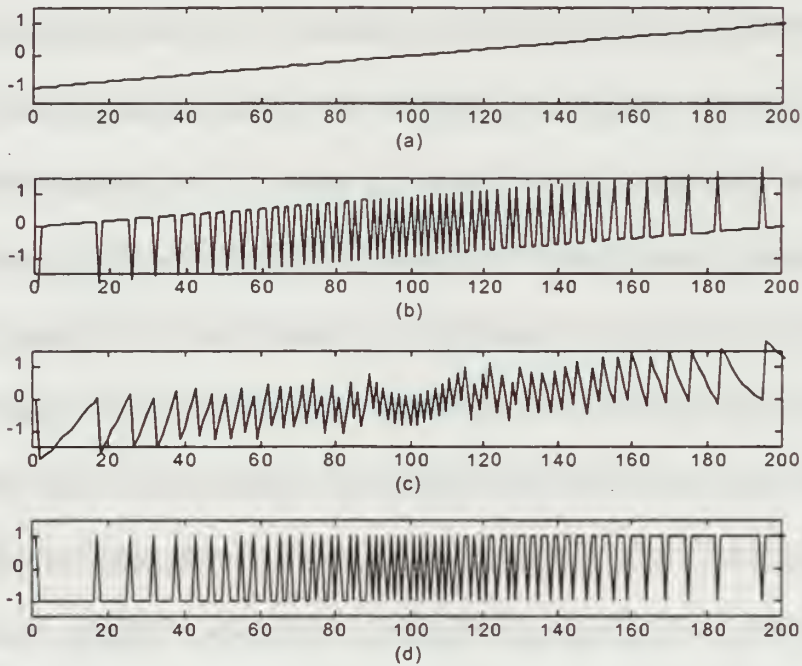


Figure 5: Electronic first-order $\Sigma\Delta$ ramp (a) input signal (b) with feedback subtracted (c) after integration/accumulation (d) comparator output.

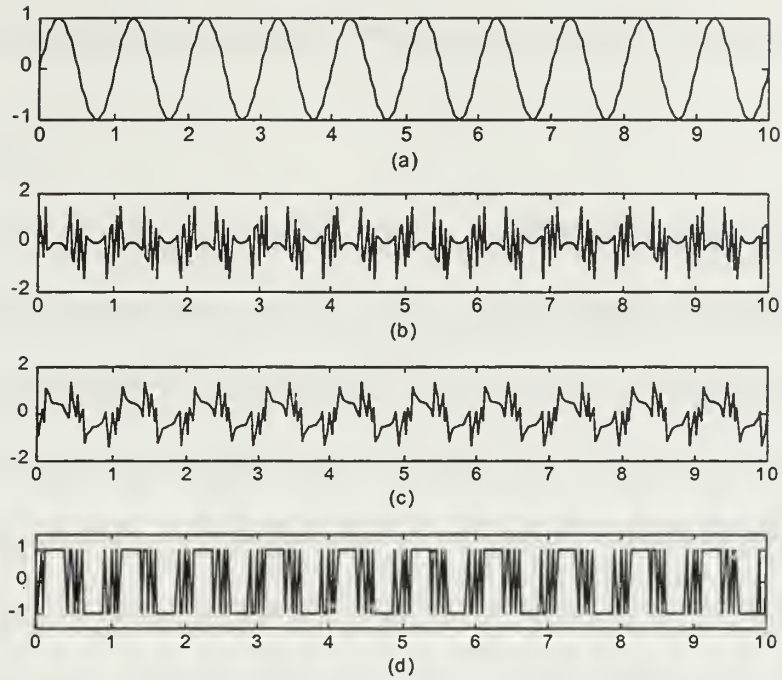


Figure 6: Electronic first-order $\Sigma\Delta$ sinusoidal (a) input signal (b) with feedback subtracted (c) after integration/accumulation (d) comparator output.

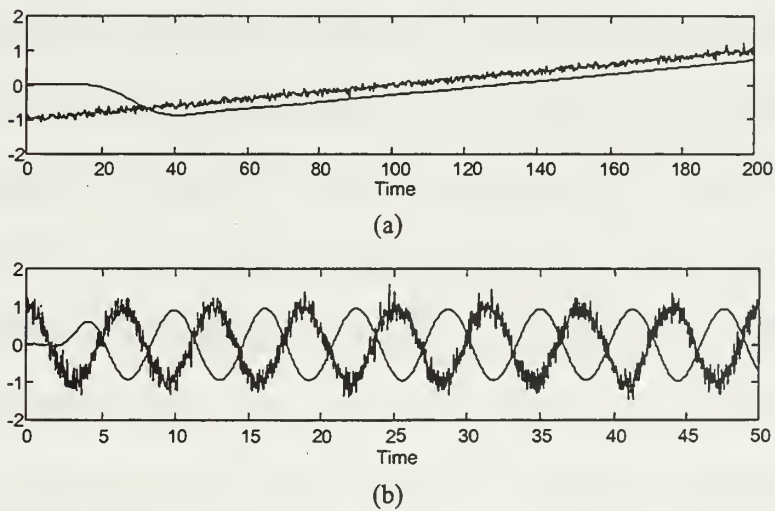


Figure 7: Electronic $\Sigma\Delta$ A/D Converter outputs for (a) a ramp signal with noise (b) a sinusoid with noise. The smooth signals are the output.

XXXXXXXXXXXXXXXXXXXX

XXXXXXXXXXXXXXXXXXXX

XXXXXXXXXXXXXXXXXXXX

XXXXXXXXXXXXXXXXXXXX

XXXXXXXXXXXXXXXXXXXX

XXXXXXXXXXXXXXXXXXXX

XXXXXXXXXXXXXXXXXXXX

XXXXXXXXXXXXXXXXXXXX

XXXXXXXXXXXXXXXXXXXX

III. INTEGRATED OPTICAL $\Sigma\Delta$ DIGITAL ANTENNAS

A. OVERVIEW

Optical oversampling ($\Sigma\Delta$) digital antennas use fiber lattice accumulators, Mach-Zehnder interferometers (MZIs), and high pulse-repetition-frequency (PRF) mode-locked lasers to oversample wideband signals directly at the antenna. As high PRF mode-locked laser technologies continue to improve (currently PRFs of 100+ GHz with time jitter <100 fs), the oversampling of wideband signals becomes increasingly feasible. This gives an advantage to optical $\Sigma\Delta$ digital antennas over contemporary all-electronic receivers. These antennas provide the ability to digitize wideband signals directly with high-resolution. The fiber lattice accumulators embedded within a feedback loop allow the time and amplitude jitter requirements of the mode-locked laser to be relaxed. Other advantages include insensitivity to vibration and electromagnetic interference, separation of the sampling mechanism from the antenna signal, and the elimination of the need to down-convert the signals before digitization. The driving force behind optical $\Sigma\Delta$ antenna technology is the large-bandwidth, high-resolution applications that are beyond the capability of the all-electronic $\Sigma\Delta$ architectures (limited typically to the audio range).

The main focus of this thesis is to present a novel fiber lattice accumulator design for integrated optical $\Sigma\Delta$ antenna technology. The fiber lattice design uses phase modulation to produce the proper interference between input optical pulses and recirculated optical pulses in order that they may be coherently combined. In this manner, the accumulation within the fiber lattice takes into account the sign of the sampled bipolar antenna signal. The fiber lattice performance is then numerically

evaluated within a first-order optical $\Sigma\Delta$ digital antenna phase coherent simulation. The errors in antenna performance as a function of the input signal are also quantified.

B. OPTICAL $\Sigma\Delta$ DIGITAL ANTENNAS

A block diagram of a first-order optical $\Sigma\Delta$ digital antenna architecture is shown in Figure 8. The corresponding computer program is shown in Appendix B, Figure B1.

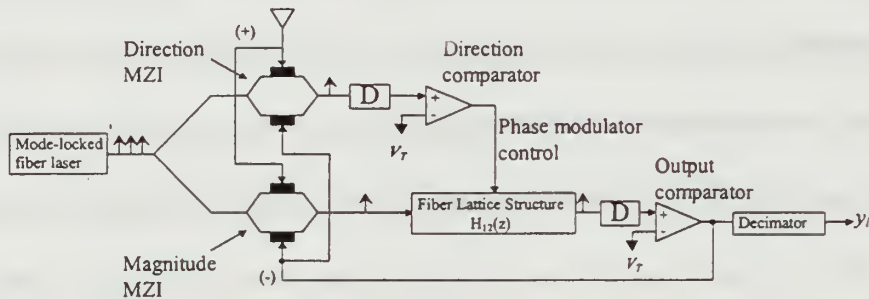


Figure 8: Integrated optical $\Sigma\Delta$ digital antenna.

The optical $\Sigma\Delta$ antenna is a phase coherent device that relies on oversampling the antenna signal directly at an MZI with a high PRF mode-locked laser. Since light intensity can only be positive, two properly phased MZIs are used to encode both the sampled antenna signal *magnitude* and polarity (the sampled signal's sign or *direction* for fiber lattice accumulation). The MZIs are also used to subtract the output comparator's feedback signal ($V_{feedback}$) from the antenna signal ($V_{antenna}$). The accumulation of the laser pulses is accomplished within the fiber lattice structure using the polarity information from the *direction* MZI. The output sample of the fiber lattice is detected and amplitude analyzed with a high-speed comparator. The decimation filter is then applied to the output comparator signal (demodulation).

C. OPTICAL COMPONENTS AND PHASE COHERENT MODELING

The following is a detailed description of the phase coherent model and individual components of the optical $\Sigma\Delta$ antenna.

1. Mode-Locked Laser

The mode locked laser is a high-rate pulsed type laser capable of oversampling antenna signals directly at the interferometers. Each individual pulse is analogous to a clock sample in an electronic ADC. The sampling characteristics of a typical mode-locked laser include PRFs between 10 and 100 GHz, pulsewidths of 0.7 ps, and a light wavelength of 1550 nm.

a. Theory and Description

In a typical laser cavity, there are many modes operating simultaneously. The relative phase of these modes is often random and incoherent causing the light from the laser to fluctuate as the modes interact constructively and destructively. Mode-locking is achieved when distinct longitudinal modes of a laser, all having slightly different frequencies, are combined in phase. The peak amplitudes of these oscillating modes, together in phase, periodically combine constructively to form a mode-locked pulse [Ref. 8].

The pulses are formed when sine waves in multiples of 2π are added in phase with one another so all their phases are zero at the same spatial locations. When added together they produce a total field amplitude. Squaring the amplitude gives the intensity and characteristic pulsed nature of a mode-locked laser pulse. A detailed analysis is found in [Ref. 8].

b. Phase Coherent Model

To model the exact parameters of a mode-locked laser on a computer is difficult due to the large amount of computer time steps required to obtain accurate results. Therefore, proportionally scaled down frequencies and pulse duty cycles, significantly lower than the actual laser operating parameters were used in the model to demonstrate the concept and correct operation of the optical $\Sigma\Delta$ digital antenna. Another consideration to insure correct operation of the optical $\Sigma\Delta$ computer model is to choose PRFs that are multiples of the computer sample time. Otherwise, the optical delay in the fiber lattice is unable to generate the correct delay.

The phase coherent mode-locked laser model is designed by simulating the electric field inside each pulse as a sinusoidal signal $A\cos\omega_L t$, where ω_L is the frequency of the laser light and A is the amplitude of the pulse. Multiplying by a rectangular pulse gives the characteristic pulsed waveform. Figure 9 shows the expanded view of a simulated laser waveform to visualize pulse design. In an actual mode-locked

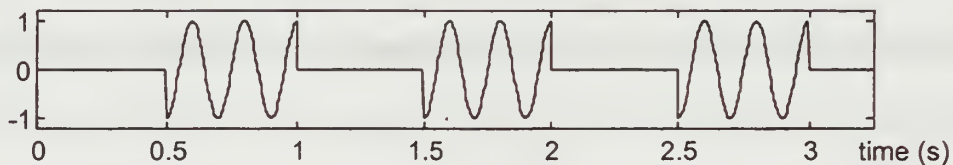


Figure 9: Output of modeled mode-locked laser.

laser, the percentage of pulse width to pulse repetition interval (pulse duty cycle) is 1% to 10% depending on sampling requirements. Scaled pulse duty cycles from 1% to 50% were successfully simulated. On the other hand, the laser light, because it's frequency is over 1000 times greater than the pulse repetition frequency (PRF), was not scaled proportionally to the actual mode-locked laser parameters because of computer

limitations. Actual model designs used PRFs from 4-100 Hz, and light frequencies from 20-400 Hz.

2. Mach-Zehnder Interferometers

The MZIs are used to efficiently couple the rf antenna signal into the optical realm, and subtract the feedback signal from the antenna signal. Figure 10 shows a

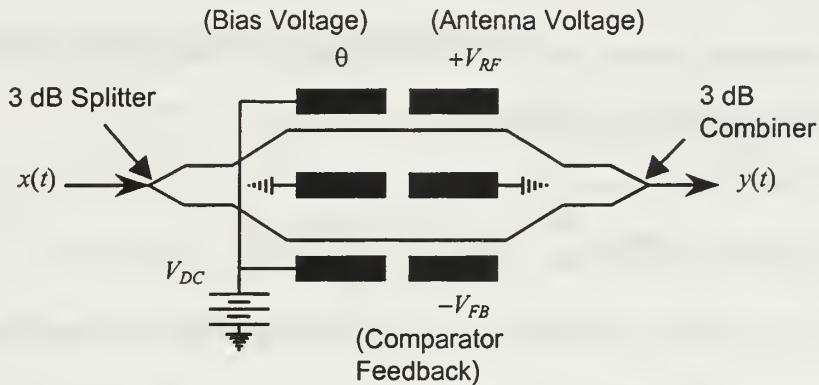


Figure 10: Schematic diagram of an MZI with different electrodes on separate paths.

general block diagram of an MZI.

a. Theory and Description

An MZI consists of a 3dB intensity splitter, two optical fiber waveguides, electrodes, and an intensity combiner. The 3dB intensity splitter separates the mode-locked laser pulses into the two separate waveguides. The electrodes, which are positioned along the optical waveguide lengths, receive the antenna, feedback and DC bias voltages that create electric fields around the optical waveguides. Both paths of the MZI are affected separately so that when the pulses are recombined at the MZI output, constructive and destructive interference occurs. The voltages are applied separately to each path with opposite polarity (push-pull) configuration. For example, the antenna voltage is applied to one waveguide and the feedback voltage is applied to the other. The

applied electric field modulates the phase of the incoming laser pulse by changing the index of refraction of the optical waveguides as a function of the voltage. The two waveguides are then recombined at the output resulting in an output laser pulse amplitude modulated by the analog voltage (constructive and destructive interference). If no voltage is applied to the electrodes, the pulses recombine coherently for the maximum output.

The output intensity of the MZI is a function of the phase difference $\Delta\phi$ between the two waveguide paths as [Ref. 13]

$$H_{MZI} = \frac{I_{out}}{I_{in}} = \frac{1}{2} + \frac{1}{2} \cos[\Delta\phi(v) + \theta] \quad (4)$$

where I_{out} and I_{in} are the output and input light intensities, respectively. The phase angle θ is a DC bias term that is used to adjust separately the quadrature point of the interferometers to create both a *magnitude* and *direction* MZI transfer function. The voltage dependent phase shift is

$$\Delta\phi(v) = \frac{2\pi n_e^3 r \Gamma L_i v(t)}{G \lambda_L} \quad (5)$$

where $v(t) = V_{antenna} - V_{feedback}$, n_e is the extraordinary index of refraction of the optical guide, r_{33} is the pertinent electro-optic coefficient, Γ is the electro-optic overlap parameter, G is the inter-electrode gap, and λ_L is the laser wavelength. In terms of v_π , the voltage required to shift the phase by π radians

$$\Delta\phi(v) = \frac{\pi v(t)}{v_\pi} \quad (6)$$

where

$$v_{\pi} = \frac{G\lambda_L}{2L_i n_e^3 r_{33} \Gamma} \quad (7)$$

For the MZIs modeled in this thesis, the laser pulsed light was assumed to be traveling in the x direction of the optical waveguide and polarized in the z direction. Therefore, the optical device is characterized as a transverse modulator vice a longitudinal modulator. This allows a smaller voltage to effect the phase change of π radians, making the device more efficient [Ref. 9].

The type of optical medium simulated in the MZI models was LiNbO₃. The optical parameters for LiNbO₃ and various other optical materials can be found in [Ref. 10]. LiNbO₃ MZIs are perfectly suited for the high bandwidth applications (40GHz) associated with the optical $\Sigma\Delta$ digital antenna.

b. Phase Coherent Model

The intensity transfer function given in Equation 4 is used to model the *direction* MZI. The *magnitude* MZI, however, requires a coherent model since the phase of the laser pulse must be preserved. This requires modeling the MZI waveguide paths separately (one as a phase modulator and the other left unaffected) to determine the modulation effects on the phase of each pulse as a function of the antenna voltage. A block diagram of the *magnitude* MZI containing a phase modulator is shown in Figure 11.

The electric field for the path of the MZI containing the phase modulator is [Ref. 10]

$$E_1 = \frac{A}{2} \cos[\omega_L t + \delta(v)] \quad (8)$$

where

$$\delta(v) = \frac{\pi v(t)}{v_\pi} \quad (9)$$

is the phase modulation term and $v(t) = V_{antenna} - V_{feedback}$ is the total signal applied to the interferometer electrodes. Rewriting,

$$E_1 = \frac{A}{2} (\cos \omega_L t \cos \delta - \sin \omega_L t \sin \delta) \quad (10)$$

allows the phase modulation due to the antenna and feedback signal to be applied to the laser pulse. The MZI output is then

$$E_{out} = E_1 + E_2 = \frac{A}{2} (\cos \omega_L t \cos \delta - \sin \omega_L t \sin \delta) + \frac{A}{2} \cos \omega_L t \quad (11)$$

where E_2 is the electric field in the other (unmodulated) waveguide path. Figure 12

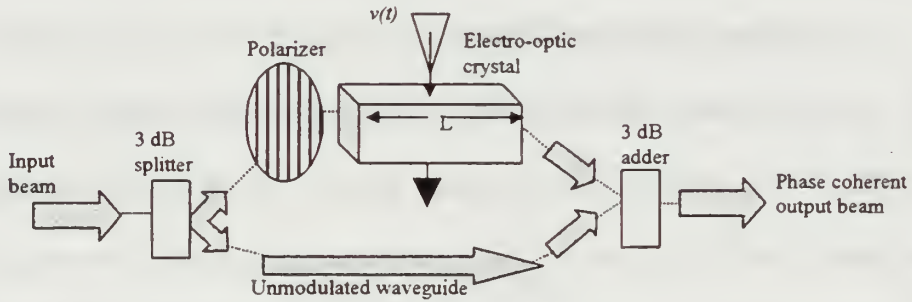


Figure 11: MZI with Electro-optic phase.

shows the intensity transfer function (Eqn. 4) for both the *direction* and *magnitude* MZIs along with the detected pulse from the phase coherent model (Eqn. 11) for an applied ramp function $-1V$ to $1V$ (pulse detection is discussed in Section C4). Note that for $v(t) > 0V$, the direction MZI detector's output voltage (corresponding to the intensity I_{out}) exceeds the *direction* comparator's voltage threshold, $V_T = 0.5$. The *direction* comparator's output voltage is used to drive the phase modulator within the fiber lattice (accumulation up or accumulation down).

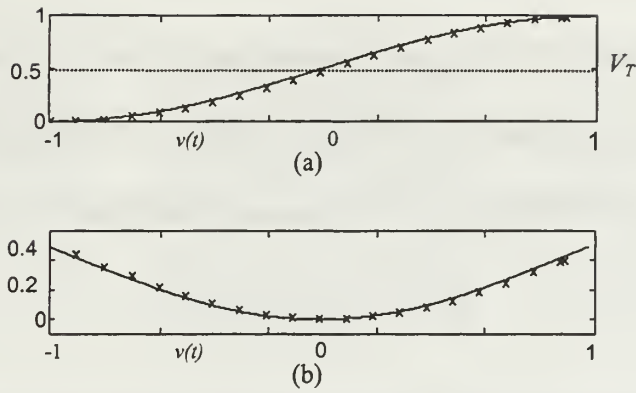


Figure 12: MZI intensity transfer functions (solid line) and phase coherent MZI detected output for (a) direction MZI and (b) magnitude MZI.

3. Fiber Lattice Structure

a. Theory and Description

The basic fiber lattice structure consists of two directional couplers, an optical amplifier, and a delay due to the length of the recirculating optical fiber. These components form the optical equivalent of the accumulator in the all-electronic $\Sigma\Delta$ architecture. The general block diagram is shown in Figure 13 [Ref. 13]. Blocks A_0 and

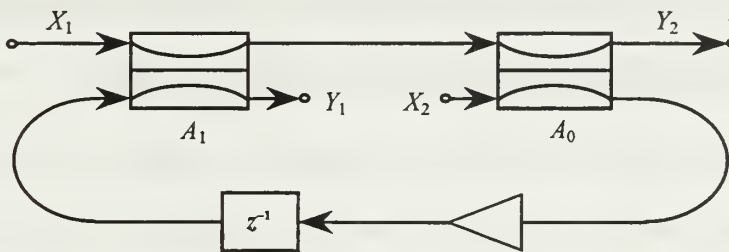


Figure 13: General Four Port Fiber Lattice Structure.

A_1 are the directional couplers, X_1 and X_2 are the input ports, Y_1 and Y_2 are the output ports, G is the optical gain block, the lines represent the optical fiber, and the z^{-1} block represents the optical sample delay (1/PRF).

By choosing different combinations of directional coupler input and output ports in the fiber lattice structure, one can select between a variety of known

transfer functions [Ref. 11]. Two such combinations reproduce the accumulator transfer functions in the all-electronic $\Sigma\Delta$ architectures (Eqns. 2, 3). Selecting the input port X_1 and output port Y_2 , while leaving X_2 and Y_1 unused, produces the transfer function

$$H_{21}(z) = \frac{(1-a_o)(1-a_1)}{1-a_o a_1 G z^{-1}}, \quad (12)$$

which can be related to Equation 2 where $A=(1-a_0)(1-a_1)G$ and $B=a_0 a_1 G$ are the gain coefficients. Inversely, selecting input port X_2 and output port Y_1 , while leaving X_1 and Y_2 unused, produces the transfer function

$$H_{12}(z) = \frac{(1-a_o)(1-a_1)G z^{-1}}{1-a_o a_1 G z^{-1}}, \quad (13)$$

which can be related to Equation 3 where $C=(1-a_0)(1-a_1)G$ and $D=a_0 a_1 G$. G is the optical amplifier gain, a_0 and a_1 are the coupling coefficients of the directional couplers, and z^{-1} is the optical sample delay. More information on stability and theory of fiber lattice structures can be found in [Refs. 11, 12]. A program to convert from all-electronic gain coefficients (A, B, C, D) to optical coefficients (a_0, a_1, G) is provided in Appendix C along with a program to compare their outputs with a specified input.

For the correct operation of the fiber lattice structure within the $\Sigma\Delta$ architecture, the directional couplers must be matched to the optical gain to produce a monotonic or linear response with a constant input. Figure 14 shows three plots of the output of the fiber lattice structure with the same constant input, but varying optical gain coefficients (G). Figure 14a shows the output of a perfectly tuned fiber lattice represented by the monotonic increase. Figure 14b shows when the gain is set too low how the accumulation rate peaks and settles at a constant value (accumulation too slow). Figure 14c shows the exponential rise associated with a gain that is too high

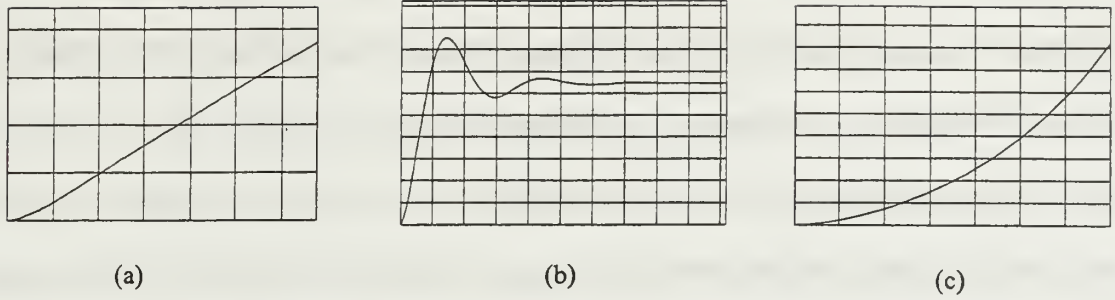


Figure 14: Output plots for fiber lattice structure $H_{12}(z)$ with a constant input showing (a) monotonic increase (b) gain too low (c) gain too high.

(accumulation too fast). A monotonic response of the fiber lattice structure is important to insure the steady accumulation, up or down, of the input signal. A table of matching values for a_0 , a_1 , and G are listed in Appendix C, Table C1 [Ref. 7]. Both fiber lattice structures, $H_{12}(z)$ and $H_{21}(z)$, use the same coefficients. As with the all-electronic accumulator, the difference between the $H_{12}(z)$ and $H_{21}(z)$ are their accumulation rates.

b. Directional Coupler Models

A directional coupler consists of two individual optical fiber waveguides of the same optical material passing through a separate optical medium. Their ability to couple light energy in specified ratios makes them a very important part of the fiber

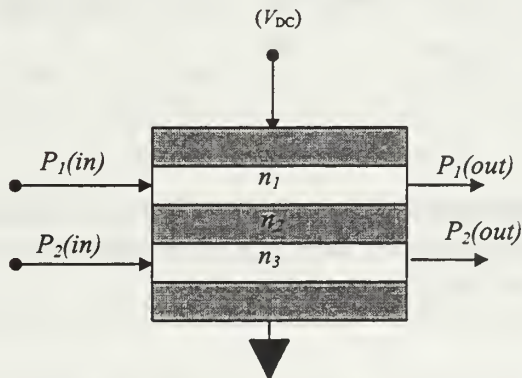


Figure 15: Schematic representation of a voltage controlled directional coupler.

lattice structure and its operation. A block diagram of a directional coupler is shown in Figure 15. The index of refraction of the optical waveguides are $n_1=n_3$. The optical medium has an index of refraction n_2 . The index of refraction of the medium (n_2) can either be fixed permanently or controlled as a function of an applied DC voltage ($n_2(V)$). The voltage creates an electric field that changes the medium's index of refraction (n_2) to equal the index of refraction of n_1 and n_3 . This enables the light energy from n_1 and n_3 to cross through the optical medium and couple into the opposite waveguide. The ratio of energy coupled is governed by the size of the electric field.

All directional couplers have two input ports and two output ports, although only three of the four in each coupler are used in the fiber lattice design application (Fig. 15). In the $H_{12}(z)$ fiber lattice, the A_0 directional coupler uses both input ports to couple the light energy into a single output. The second output port is terminated. The A_1 directional coupler uses one input and two outputs. The A_0 and A_1 coupler models for the $H_{21}(z)$ accumulator are reversed in the $H_{12}(z)$. Figure 16 shows the directional coupler models used in the $H_{21}(z)$ and $H_{12}(z)$ accumulator designs.

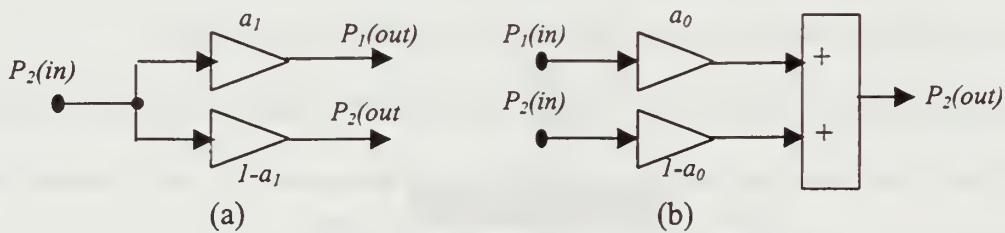


Figure 16: Block diagrams of the (a) A_1 and (b) A_0 directional coupler computer models for the $H_{12}(z)$ fiber lattice structure. The A_1 and A_0 are interchanged for the $H_{21}(z)$.

The coupling coefficients (a_0, a_1) in the fiber lattice transfer function control the energy coupling amount within the fiber lattice model. They calculate the

scaled amplitude of the incoming pulse to the amount that would in reality couple to the opposite waveguide. For example, in Figure 16b, if $a_0 = 0.4$ in the A_0 coupler, then 40 % of the light energy entering $P_1(in)$ will couple to the P_2 waveguide. Proportionally, in the second waveguide (P_2), $1 - a_0$ must equal 0.6, and therefore 60% of it's entering light energy will remain in the P_2 waveguide to add coherently to the 40% coupled from the P_1 waveguide. In this particular example, only the P_2 waveguide output is required, and the other is terminated. The SIMULINK program model of the directional couplers is shown in Appendix B, Figure B4. Different ratios for a_0 and a_1 can be chosen with each set linked to a specific gain (G) in order for the fiber lattice device to operate monotonically (Appendix C, Table C1).

c. Phase Coherent Model

The phase coherent model of the optical $\Sigma\Delta$ accumulator consists of a phase modulator positioned at the input of the fiber lattice structure. The schematic diagram of the phase coherent $H_{12}(z)$ fiber lattice is shown in Figure 17. Optical

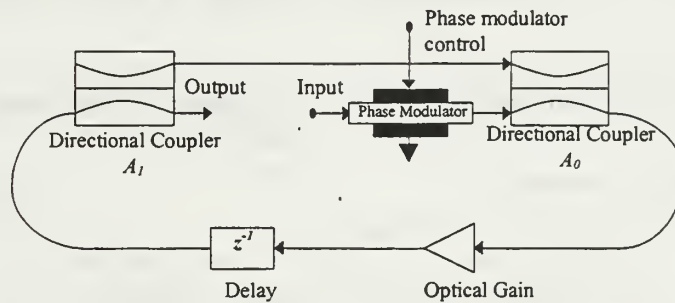


Figure 17: Schematic diagram of the fiber lattice structure with recoupling phase modulator at the input.

coefficients used to optimize the fiber lattice in this thesis were $a_0 = 0.6$, $a_1 = 0.4$ and $G = 4.16$. Only a first-order optical $\Sigma\Delta$ digital antenna (Fig. 8) is presented in this thesis in which only the $H_{12}(z)$ fiber lattice structure is utilized.

The phase modulator within the fiber lattice recouples the *direction* and *magnitude* MZI outputs so the correct accumulation of the signal within the fiber lattice occurs. This is accomplished by phase modulating the fiber lattice input signal (*magnitude* MZI output) depending on the *direction* MZI comparator voltage (Fig. 8). That is, if the detected intensity voltage from the *direction* MZI exceeds the *direction* comparator voltage threshold, $V_T=0.5$, the *direction* comparator output voltage selected is $\sigma = 0V$. Otherwise the *direction* comparator output voltage to the fiber lattice phase modulator is $\sigma = v_\pi$, the voltage required to phase shift the *magnitude* MZI output by π .

To calculate the output of the fiber lattice phase modulator, the magnitude MZI output (Eqn. 11), is first rewritten as

$$E_{out} = E_1 + E_2 = \text{Re}\left[e^{j(\omega_L t + \delta)} + e^{j\omega_L t}\right]. \quad (14)$$

The output of the fiber lattice phase modulator (E_ϕ) is then calculated by multiplying Equation 14 by the *direction* comparator output so that

$$E_\phi = \text{Re}\left[\left(e^{j(\omega_L t + \delta)} + e^{j\omega_L t}\right)e^{j\frac{\pi}{v_\pi}\sigma}\right] \quad (15)$$

where $\sigma = 0$ or v_π . The real part of Equation 15, the output of the fiber lattice phase modulator, can then be written as

$$E_\phi = \left[\cos \omega_L t \cos\left(\delta + \frac{\pi}{v_\pi}\sigma\right) - \sin \omega_L t \sin\left(\delta + \frac{\pi}{v_\pi}\sigma\right) \right] + \left[\cos \omega_L t \cos \frac{\pi}{v_\pi}\sigma - \sin \omega_L t \sin \frac{\pi}{v_\pi}\sigma \right]. \quad (16)$$

If $\sigma=0$, then no modulation of the *magnitude* MZI signal occurs, and both the input pulse and the recirculating pulse enter the A_0 directional coupler (Fig. 17) and combine

coherently (addition). If $\sigma = \nu\pi$, then the input signal from the *magnitude* MZI receives a phase shift of π and the two pulses add destructively (subtraction).

4. Output Photodetector

When the light exits the fiber lattice structure, it is a simulation of the electric field in the phase altered laser pulse. The output light must be detected and converted into a voltage. To model a photodetector, the first step is to square the output pulses as they exit the fiber lattice to determine their intensity. Next, each pulse is integrated individually. The signal's envelope is then calculated to determine the detector output voltage. The integration can be expressed as

$$V(\Delta t) = I(\Delta t) = \int_{t_1}^{t_2} E_{pulse}^2(t) dt \quad (17)$$

where E_{pulse} is the electric field of the phase modulated output pulse from the fiber lattice, $V(\Delta t)$ is the average detected voltage, $I(\Delta t)$ is the average pulse intensity, and Δt is the pulse length. A block diagram of the photodetector model is shown in Figure 18. The SIMULINK model is shown in Appendix B, Figure B5.

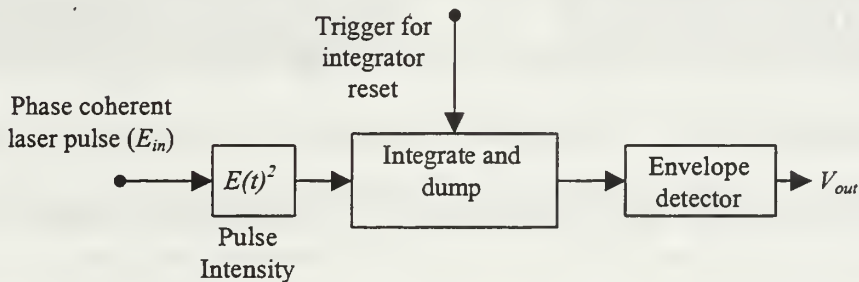


Figure 18: Block diagram of photodetector model.

5. Output Comparator

The detected fiber lattice output signal modulates the output comparator. If the detected fiber lattice output intensity is greater than 0.5, the comparator state $V_{feedback} = 1V$, otherwise the output comparator voltage $V_{feedback} = -1V$. The feedback voltage is then subtracted from the antenna signal, $v(t) = V_{antenna} - V_{feedback}$, at both the *direction* and *magnitude* MZIs.

6. Decimation Filtering

Decimating the modulated output to obtain the high-resolution digital signal is accomplished in the same way as the all-electronic $\Sigma\Delta$ architecture (lowpass filtered and then resampled at the Nyquist rate). The only consideration prior to decimation is the simulated sample rate of the laser pulses (PRF) is significantly less than the computer time steps required to efficiently run the program. For example, if the PRF of the laser is 5 Hz and the simulated light frequency within each pulse is 20 Hz, the *minimum* amount of computer time steps required to generate each pulse would be at the Nyquist rate (40 Hz) of the light frequency. Therefore, after modulation, the computer time steps must be down-sampled to equal the PRF of the laser prior to decimation, otherwise, the computer calculated decimation function will assume the time steps to be the PRF and will not calculate the output correctly. Following down-sampling, the normal decimation (lowpass filter and resample) is calculated as in the all-electronic output described in Chapter II.

D. RESULTS FOR FIRST ORDER DESIGN

Results for the optical $\Sigma\Delta$ digital antenna are compared with the all-electronic processor in Figures 19 and 20. Figures 19a and 20a show both the ramped and

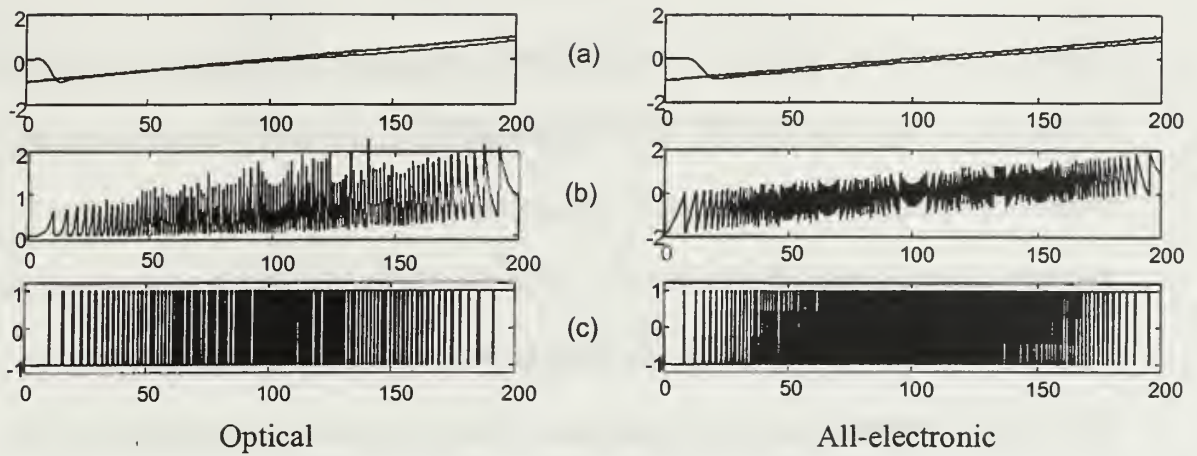


Figure 19: Comparison plot of a ramp function. Each plot shows a corresponding stage in the $\Sigma\Delta$ architectures. (a) Input ramp plotted with output. The lowpass filter during decimation creates the step function at the beginning of the output signal due to capacitor charging. (b) Output of accumulator/integrator. (c) Modulated signal at output of comparator.

sinusoidal input antenna signals and the corresponding output signals. The initial step response at the beginning of the ramped output and the phase delay in the sinusoidal

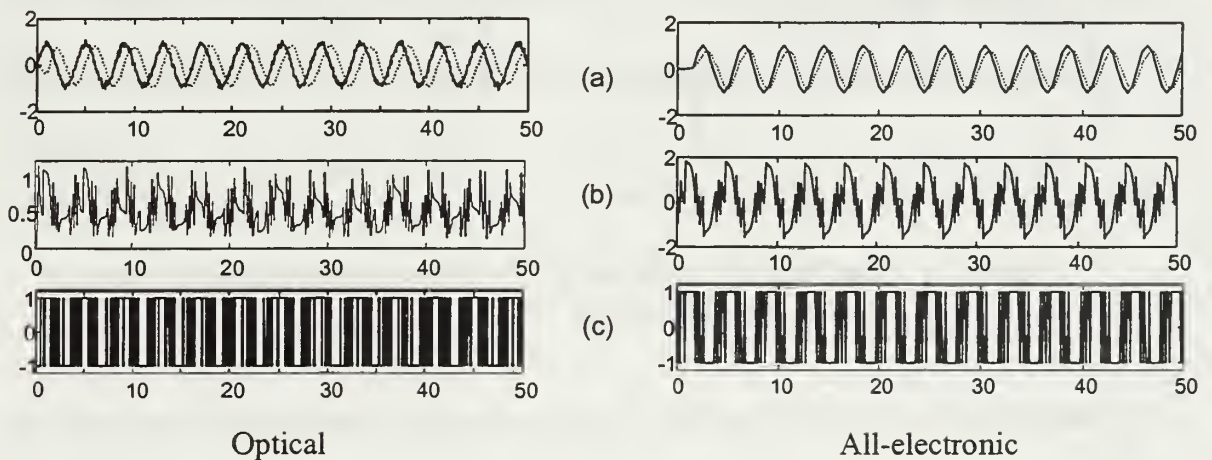


Figure 20: Comparison plot of a ramp function. Each plot shows a corresponding stage in the $\Sigma\Delta$ architectures. (a) Input sinusoid plotted with output (dashes). (b) Output of accumulator/integrator. (c) Modulated signal at output of comparator.

output are due to the lowpass filter initial charge-up during decimation. The output of the accumulator stage (Figs. 19b, 20b) and output comparator stage (Figs. 19c, 20c) are also shown for comparison. The ramp signal was oversampled with a laser PRF = 4 Hz with

a duty cycle of 50%. The sinusoid signal (1/4 Hz) was oversampled with the laser PRF = 20 Hz with a duty cycle of 50%. The higher the PRFs in the optical model and clock sample times in the all-electronic architecture, the faster the modulation about the average antenna signal value decreasing visual plot clarity. For this reason, as well as increased computer time steps (as discussed in Sections C1 and C6) results using low PRFs and oversampling ratios (OSRs) were calculated and are shown so that a visual comparison of the optical $\Sigma\Delta$ architecture results can be made with the associated all-electronic design. Figure 21 shows a spectral comparison of the optical and all-electronic

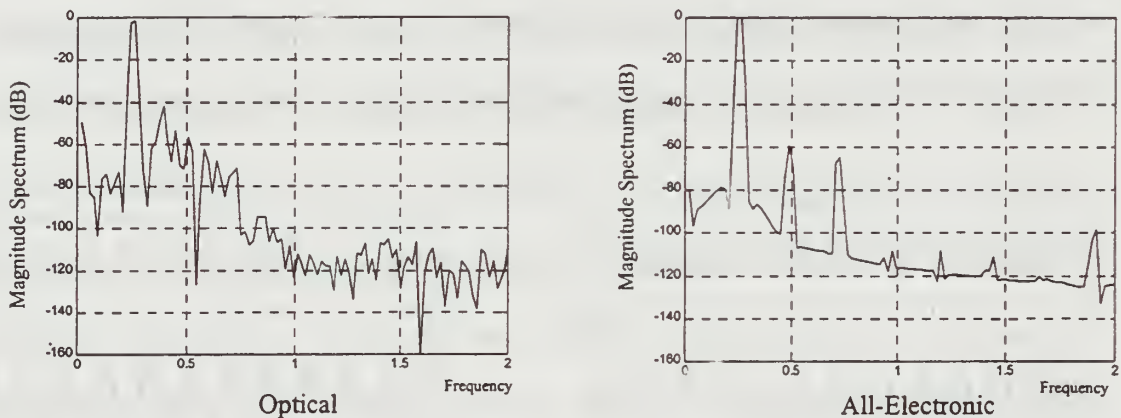


Figure 21: Fast Fourier Transform (FFT) of the optical and all-electronic $\Sigma\Delta$ outputs from Figure 20a.

$\Sigma\Delta$ output results shown in Figure 20a. The extra frequency peaks clearly seen in the all-electronic spectrum are the tones associated with the first-order design.

Figure 22 shows the error signal for the optical $\Sigma\Delta$ digital antenna simulation. The error signal is calculated as the time-domain difference between the input antenna signals and the output digital signal for both the ramp (Fig. 22a) and the sinusoid (Fig. 22b).

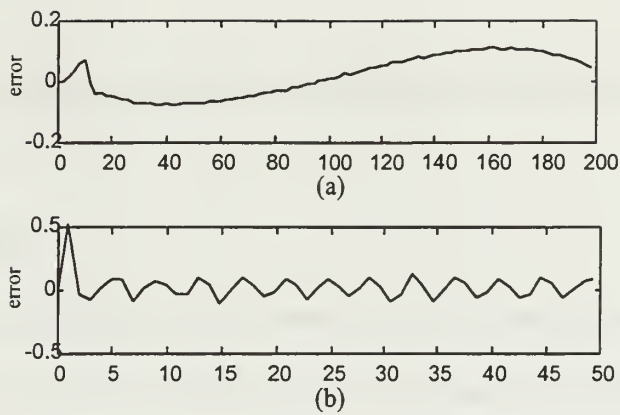


Figure 22: Error difference between the input signal and the output signal for a (a) ramp and a (b) sinusoidal signal.

E. CONCLUSION

Simulating the phase coherent nature of the optical $\Sigma\Delta$ design, a working/reliable computer model was developed. All simulation results confirm the correct operation of the integrated optical model in comparison to the all-electronic design. With sampling rates from the mode-locked laser expected to be 100 GHz, oversampling ratios of 1000 or more are expected for signal digitization in the microwave range using this optical $\Sigma\Delta$ architecture.

IV. LIMITATIONS, CONCLUSIONS, AND RECOMMENDATIONS

A. LIMITATIONS

Although the computer models were successful, certain parameters associated with the realities of this type of device were not addressed or simulated. These include signal losses associated with the optical fiber and components, undesired crosstalk within the directional couplers, mode-locked laser jitter, the length of optical fiber required to effect the proper optical delay within the fiber lattice accumulator, and the length of fiber required for the optical amplifier. The laser jitter can be added to the already developed program by programming Gaussian noise to vary the pulse length and amplitude.

Limitations with the computer program also effect the testing and results if not considered prior to running simulations. The computer program requires the simulated PRF of the mode-locked laser to be a multiple of the computer time step. Otherwise, the optical sample delay calculation in the fiber lattice structure becomes quickly inaccurate, resulting in improper constructive and destructive interference with a loss of output signal. Programming the actual parameters of a mode-locked laser is not very practical on a computer due to the tremendous amount of computer time steps required to create an accurate result. Therefore, all mode-locked laser parameters were scaled down to values that could be easily handled by the computer. This method still demonstrated the correct concept of an optical $\Sigma\Delta$ digital antenna.

B. CONCLUSIONS

Simulating the phase coherent nature of the optical $\Sigma\Delta$ design, a working/reliable computer model was developed. All simulations were developed with the software

MATLAB and SIMULINK. The results confirm the correct operation of the integrated optical model in comparison to the all-electronic design. The phase modulator fiber lattice design demonstrated the ability to properly couple and accumulate the magnitude and polarity signal information within the first order $\Sigma\Delta$ device. Only low frequency signals were used to demonstrate the optical $\Sigma\Delta$ presented in this thesis. However, the theory and concepts clearly demonstrate the optical $\Sigma\Delta$ digital antenna will work in the microwave signal band.

In conclusion, the optical $\Sigma\Delta$ digital antenna has the ability to digitize analog signals. Due to the high pulse rates associated with the mode-locked laser this could lead to direct digitization of microwave signals at significantly high oversampling ratios (OSRs) resulting in increased signal resolution and improved sensor sensitivity.

C. RECOMMENDATIONS

Further efforts include the continued optimization of the first-order integrated optical model, as well as, expansion to a second-order model (better behaved limit cycles). A block diagram of the proposed second-order optical $\Sigma\Delta$ digital antenna is shown in Appendix D. An analysis of the laser jitter effects needs to be completed in order to verify the expected relaxed jitter requirements predicted with the $\Sigma\Delta$ architecture. Also, a signal analysis needs to be modeled and conducted on the oversampled all-electronic and optical $\Sigma\Delta$ outputs at various oversampling ratios (OSRs) to show the increased signal-to-noise (SNR) and bit resolution obtained using the $\Sigma\Delta$ filter theory.

APPENDIX A: ALL-ELECTRONIC $\Sigma\Delta$ SIMULINK PROGRAM MODELS

This appendix shows the first- and second-order all-electronic $\Sigma\Delta$ SIMULINK models, their associated subsystems and a users guide to setup and run the program. The second-order results in the time domain are also shown.

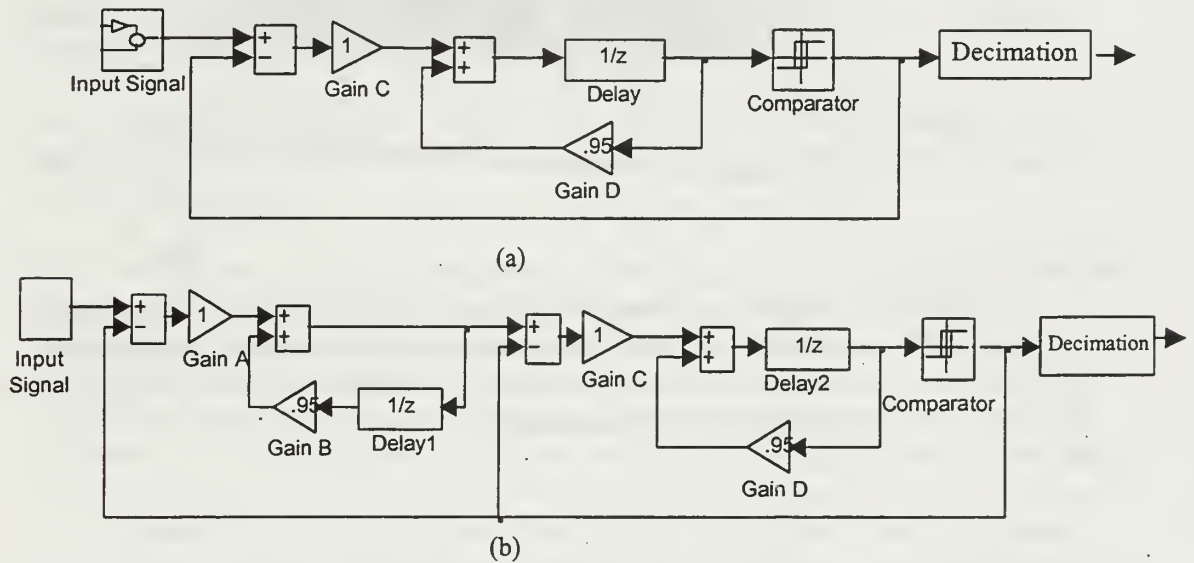


Figure A1: SIMULINK models of the all-electronic (a) first-order and (b) second-order $\Sigma\Delta$ ADCs (Files: *all-elect1.mdl*, *all-elect2.mdl*).

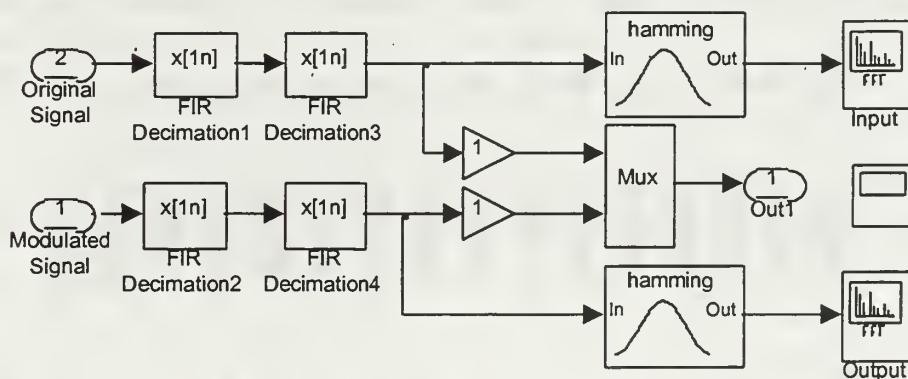


Figure A2: SIMULINK subsystem (Fig. A1) model for decimation and FFT Analysis of modulated signals

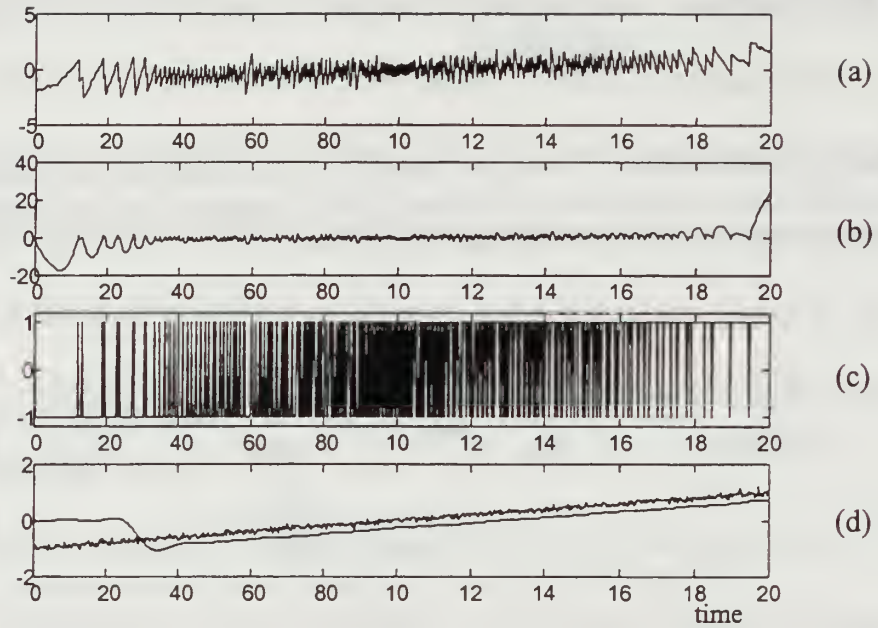


Figure A3: Output results for a second-order all-electronic $\Sigma\Delta$ ADC with a ramped input. (a) First stage accumulator output, (b) second stage accumulator output, (c) modulated output, (d) input (noisy) plotted with digitized output.

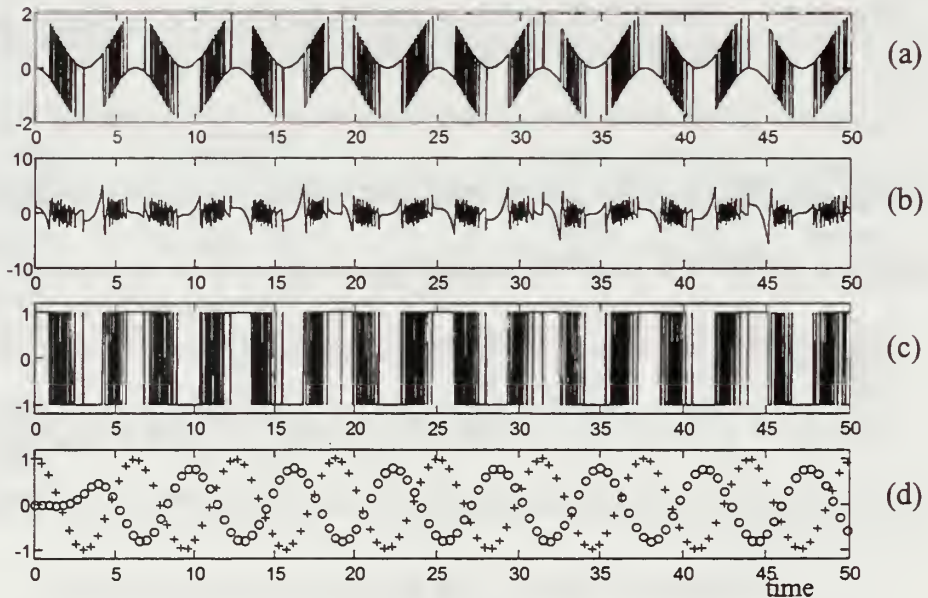


Figure A4: Output results for a second-order all-electronic $\Sigma\Delta$ ADC with a sinusoidal input. (a) First stage accumulator output, (b) second stage accumulator output, (c) modulated output, (d) input (+) plotted with digitized output.

USER'S GUIDE FOR ALL-ELECTRONIC $\Sigma\Delta$ ADC SIMULINK MODEL

1. Select from the SIMULINK library the type of antenna signal to be digitized. Enter in signal parameters and connect in place of the "Input Signal" block in Figures A1a or A1b.
2. Select "Gain" parameters. The ideal for both models is to set all gain parameters to 1.
3. Set all sample "Delay" blocks to $1/f_s$, where f_s is the sampling frequency of the system. The sampling frequency is also the computer time step rate at which the overall program is set to run.
4. The "Comparator" (Figs. A1a, A1b) is a SIMULINK relay function block. The threshold is set at 0. It should be set to output a "1" when the block is "on" and a "-1" when the block is off.
5. The "Decimation" SIMULINK subsystem block (Figs. A1a, A1b) lowpass filters and resamples the signal to remove the modulation and out-of-band noise. It also calculates the FFT for the input and output signals for comparison. Both models use the same decimation subprogram (Fig. A2). The "FIR decimation" for the input signal downsamples the original oversampled signal to the Nyquist rate. The "FIR Decimation" block parameters for the input and modulated signal should be the same. The "sample time" is $1/f_s$. The "decimation factor" is the integer amount the signal is to be downsampled. Avoid downsampling factors greater than 8 due to program inaccuracies. Instead use multiple decimation blocks in series. The lowpass filter is a "fir1". Filter orders of 15-25 are sufficient for sinusoidal signals.
6. Following decimation, the signal can either be viewed in the time-domain or the frequency domain. In the frequency domain, a "Hamming" window function block and "Buffered FFT Scope" are used with parameters:
 - a. Parameters typically used for the Hamming window function were: Window length=128 with periodic sampling.
 - b. Parameters typically used for the buffered FFT scope were: Buffer size-128, Buffer overlap-64, FFT length-128, sample time- $1/f_n$, where f_n equals the Nyquist frequency.

APPENDIX B: OPTICAL $\Sigma\Delta$ SIMULINK PROGRAM MODEL

This appendix shows the entire SIMULINK optical $\Sigma\Delta$ program design, it's associated subsystems, and a users guide to setup and run the program.

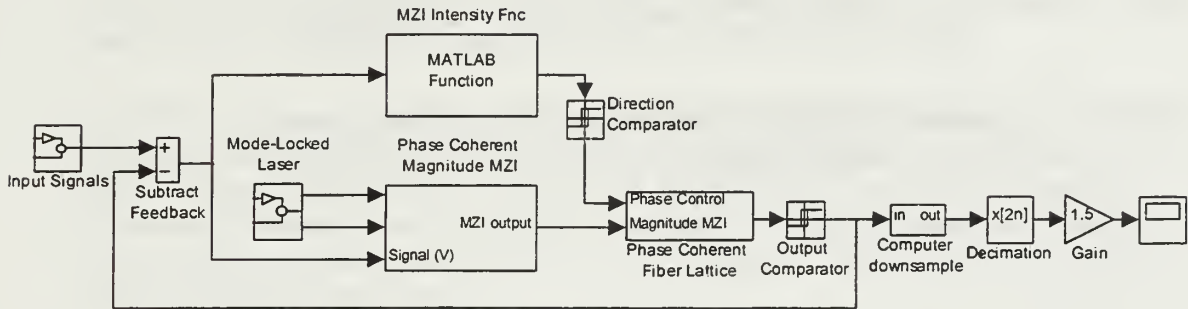


Figure B1: SIMULINK program model for the integrated optical $\Sigma\Delta$ digital antenna. (File: optical1.mdl)

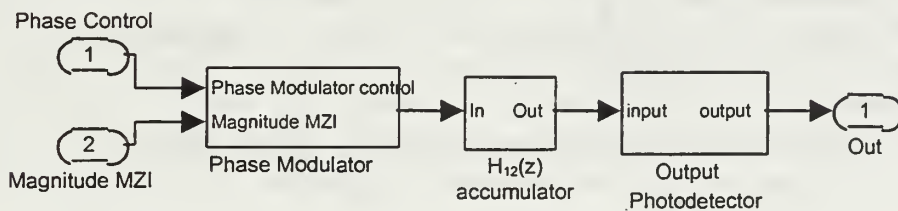


Figure B2: SIMULINK subsystem model of the “Phase Coherent Fiber Lattice” (Fig.B1).

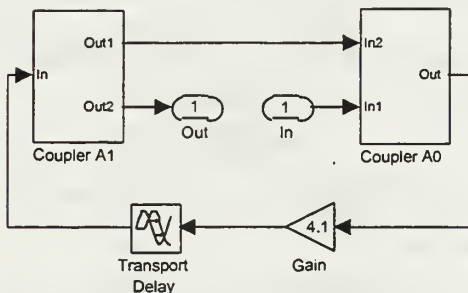


Figure B3: SIMULINK subsystem model of “ $H_{12}(z)$ Accumulator” (Fig. B1)

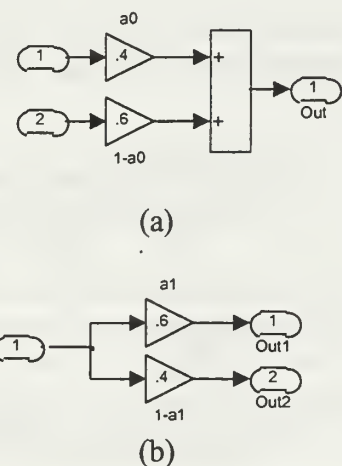


Figure B4: SIMULINK subsystem models of the $H_{12}(z)$ directional couplers (a) A_0 and (b) A_1 (Fig. B3).

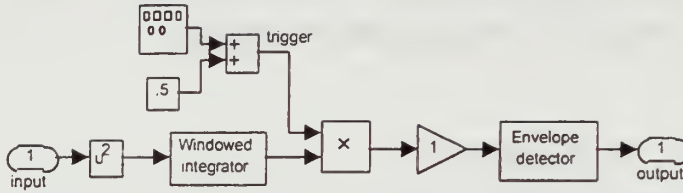


Figure B5: SIMULINK subsystem model the “Photodetector” design (Fig. B2)

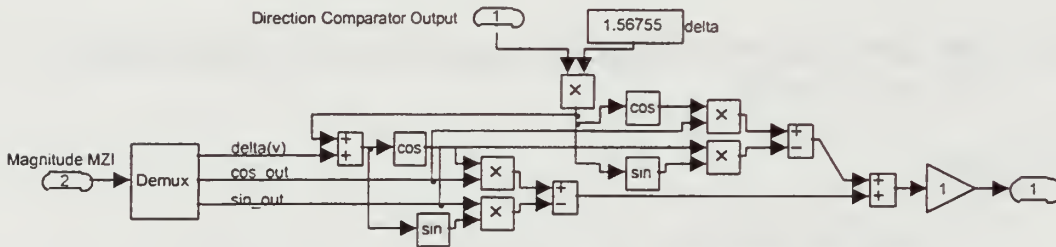


Figure B6: SIMULINK subsystem model of the fiber lattice “Phase Modulator” (Fig B2). Represents Equation 16.

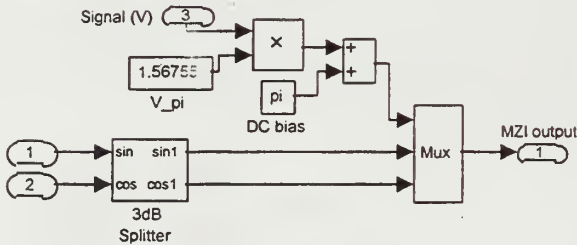


Figure B7: SIMULINK subsystem model of the “Phase Coherent Magnitude MZI” (Fig. B1).

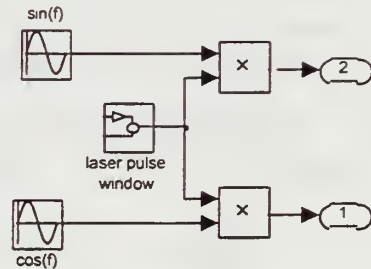


Figure B8: SIMULINK subsystem model of the “Mode-Locked Laser” (Fig. B1)

USERS GUIDE FOR OPTICAL $\Sigma\Delta$ SIMULINK MODEL

1. Select from SIMULINK the type of antenna signal to be digitized. Enter in desired parameters and connect in place of the “Input Signal” block in Figure B1
2. Go to the “Mode-Locked Laser” subsystem block (Fig. B1) select the laser PRF in the block “Laser Pulse Window”(Fig. B8). Next, choose a light frequency and enter into the “sin(f)” and “cos(f)” function blocks.
3. The MATLAB Function block labeled “MZI Intensity Fnc” (Fig. B1) is a MATLAB function, The name of the MATLAB function should be entered in the SIMULINK block. The program code is in Appendix E, Program E2. The program should not require any changes unless the optical properties of the MZI are changed. Because it is the intensity transfer function, the only input required is the antenna signal with feedback already subtracted.
4. The “Phase Coherent Magnitude MZI” SIMULINK subsystem (Fig. B1) has the two laser outputs as it’s inputs along with the antenna signal with feedback subtracted. Because the laser sinusoidal components (cosine and sine) are required to be separated in order to calculate the second phase modulation prior to the fiber lattice (Fig. B7), only $\delta(\nu)$ is calculated and the rest is carried over to the fiber lattice phase modulator to perform the whole calculation at once before the signal enters the fiber lattice (Eqn. 16, Chapt. III). Appendix F shows the SIMULINK programs of the phase coherent MZI outputs of both the magnitude and direction MZIs for comparison to the MZI intensity transfer function.
5. The “Direction Comparator” (Fig. B1) is a SIMULINK relay function block. The threshold should be set at 0.5. It should be set to output “0” when the block is “on” and a “1” when the block is “off”.
6. The “Phase Coherent Fiber Lattice” SIMULINK subsystem (Fig. B1) consists of the “Phase Modulator”(Fig. B6), “ $H_{12}(z)$ Accumulator”(Fig. B3), and the “Photodetector” (Fig. B5) SIMULINK subsystems (Fig. B2).
 - a. No changes in the phase modulator are required unless a change in the optical parameters is desired. The value for ν_π should be entered in the box labeled “delta” (Fig. B6).
 - b. The “Gain” in the accumulator subsystems (Fig. B3) must be matched to the directional couplers. The directional couplers are shown in Figure B4. Go to Appendix C, Table C1 and select the coefficients a_0 , a_1 , and G . Enter these into the models in Figures B3 and B4. Never use the maximum gain given in Table C1, but operate between 0.01 and 0.1 below G or the optical circuit will tend to overload.
 - c. The SIMULINK subsystem of the photodetector is shown in Figure B5. The trigger frequency block is the same as the PRF set in the “Mode-Locked Laser”

block. The “Windowed Integrator” should have an “Input vector size” of “1” and an “Integration window length”

$$WL = \frac{1}{2(PRF)}. \quad (A1)$$

The “Sample time” is the computer time steps and the “Method” of integration is “First Order”. The “Envelope Detector” block is set to detect the “upper” boundary side.

7. The “Output Comparator” (Fig. B1) is a SIMULINK relay function block. The threshold should be set at 0.5. It should be set to output “1” when the block is “on” and a “-1” when the block is “off”.
8. The “Computer Downsample” SIMULINK block (Fig. B1) is used to downsample the computer time steps to match the PRF prior to decimation. In each block, enter the input sample time and the downsampled integer factor. Downsampling by factors greater than 8 with one function block should be avoided due to inaccuracies in the program. Therefore, multiple blocks are used.
9. The “Decimation” SIMULINK function block (Fig. B1) lowpass filters and resamples the signal to remove the modulation and out-of-band noise. The input sample time is equal to the PRF. The decimation factor is the required factor to downsample the oversampled signal at the Nyquist rate. As with the downsample block, downsampling factors greater than 8 should be avoided. Again, use multiple blocks in series. The lowpass filter type is “fir1”. Filter order of 15-25 is sufficient for sinusoidal signals.
10. The “Gain” function block (Fig. A1) is to increase the output signal after filtering and the scope is to view the output digitized signal in the time-domain.

APPENDIX C: PROGRAMS FOR COMPARISON OF THE ALL-ELECTRONIC AND OPTICAL ACCUMULATORS

This appendix shows the programs used to convert between the optical and all-electronic coefficients for comparison and contrast of the optical and electronic accumulators.

```
%File: coef_calc.m
%While loop to do repeated calculations
pick=1;
while pick==1
    fprintf('Convert from optical to electronic or vice versa?\n');
    fprintf('1-Convert from electronic to optical coefficients.\n');
    fprintf('2-Convert from optical to electronic coefficients.\n');
    choice=input('Pick one: ');

    %If know values for electronic and want to see how compares to optical
    if choice==1
        C=input('Enter numerator coefficient for H21 or H12: ');
        D=input('Enter denominator coefficient for H21 or H12: ');

        CD=C/D;
        fprintf('Choose which value to fix\n');
        fprintf('1 - fix a0\n');
        fprintf('2 - fix a1\n');
        choose=input('Pick one: ');

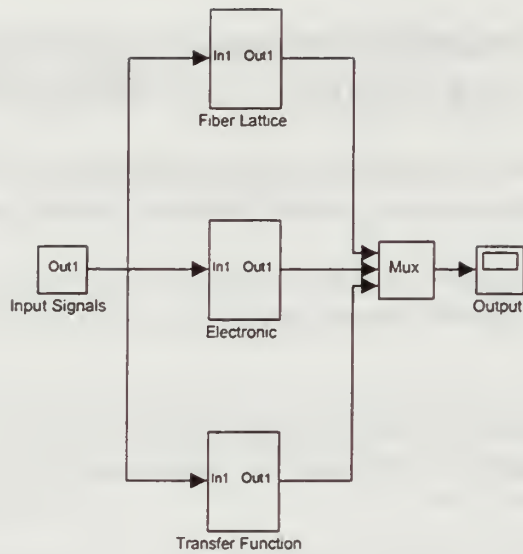
        %Must choose one of the directional coupler coefficients to solve
        equation
        if choose==1
            a0=input('Choose a coefficient for a0 (0-->1): ');
            a1=1/((CD*a0/(1-a0))+1)
            G=D/(a0*a1)

        elseif choose==2
            a1=input('Choose a coefficient for a1 (0-->1): ');
            a0=1/((CD*a1/(1-a1))+1)
            G=D/(a0*a1)
        end

        %If you know optical coefficients and want to compare to electronic
        coefficients
        elseif choice==2
            a0=input('Enter coefficient for a0(0-->1): ');
            a1=input('Enter coefficient for a1(0-->1): ');
            G=input('Enter Value for Gain (G): ');

            C=(1-a0)*(1-a1)*G
            D=a0*a1*G
        end
        pick=input('Type 1 to repeat or 2 to quit: ');
    end
end
```

Program C1: MATLAB program used to convert the electronic accumulator model coefficients to their associated optical coefficients, and vice versa.



Program C2: SIMULINK program to compare and contrast the optical fiber lattice and electronic accumulators along with their transfer function. Use program C1 to calculate coefficients. Use any input signal. (File: integrators.mdl)

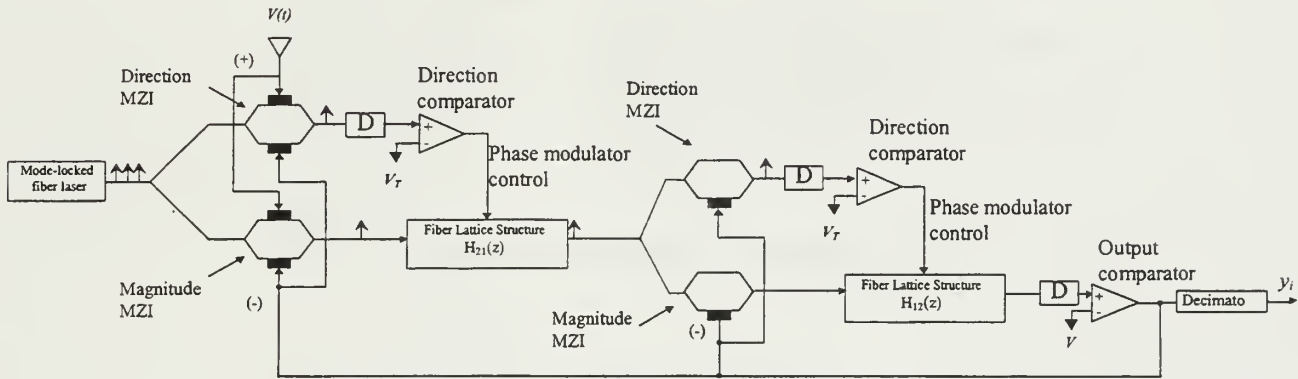
Coupling ratio, a_0

	0.1	0.2	0.3	0.4	0.5	0.6	0.7	0.8	0.9
0.1	100	50	33.33	25	20	16.66	14.28	12.5	11.1
0.2	50	25	16.65	12.5	10	8.33	7.15	6.25	5.55
0.3	33.33	16.68	11.11	8.33	6.67	5.55	4.76	4.166	3.703
0.4	25	12.5	8.34	6.25	5	4.166	3.57	3.125	2.78
0.5	20	10	6.68	5	4	3.33	2.85	2.5	2.22
0.6	16.66	8.33	5.55	4.17	3.33	2.78	2.38	2.08	1.85
0.7	14.28	7.14	4.76	3.57	2.86	2.38	2.04	1.785	1.587
0.8	12.5	6.25	4.16	3.125	2.5	2.08	1.785	1.563	1.388
0.9	11.1	5.56	3.7	2.78	2.22	1.852	1.588	1.389	1.234

Table C1: Matched optical coefficients for monotonically increasing response in the fiber lattice structure. By selecting a coupling ratio set, the correct optical gain (G) can be found for fiber lattice monotonic operation.

APPENDIX D: PHASE COHERENT SECOND-ORDER OPTICAL $\Sigma\Delta$ DIGITAL ANTENNA

This appendix shows the proposed second order $\Sigma\Delta$ digital antenna



Mathematical Analysis

Chapter 1: Introduction

1.1. Real Numbers

1.2. Limits

1.3. Continuity

Chapter 2: Derivatives

2.1. Definition of Derivative

2.2. Rules of Differentiation

2.3. Applications of Derivatives

2.4. Higher Order Derivatives

2.5. Taylor's Theorem

APPENDIX E: MACH-ZEHNDER INTERFEROMETER MAGNITUDE AND DIRECTION PROGRAMS

This appendix shows two separate programs, one MATLAB (Prog. E1) and one SIMULINK (Prog. E2) that model the MZI *direction* and *magnitude* intensity transfer functions (Eqn. 9).

```
% File: infplot.m
G = 3.0e-6;           %inter-electrode gap (m)
lambda = 0.9e-6;     %free space optical wavelength (m)
n = 2.205;           %index of refraction
r = 30.8e-12;        %electro-optic coefficient (v/m)
gamma = 1;           %overlap integral
L = 0.0020;          %length (m)

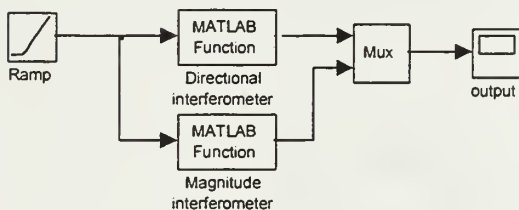
phase = pi;
dphi = (2*pi*n^3*r*gamma*L)/(G*lambda);

v = -1.5:.04:1.5;

Imag = (0.5+0.5*cos(dphi*v+phase));
Idir = (0.5+0.5*cos(dphi*v-phase/2));

plot(v, Imag, 'o')
hold
plot(v, Idir, '+')
axis([-1.5 1.5 0 1])
xlabel('Normalized Input Signal (Volts)')
ylabel('Normalized input Intensity')
%gtext('Direction')
%gtext('Magnitude')
hold
```

Program E1: MATLAB program used to illustrate the MZI *direction* and *magnitude* transfer functions.



```
% File: inferplot.mdl
function I_out=interfer(v)

G=3.0e-6;           % Inter-elect gap (m)
wl=1.5e-6;         % Wavelength (m)
n=2.205;           % Index of refraction
r=30.8e-12;        % E-Opt coef (v/m)
GAMMA=1.7;         % Overlap integral
L=0.0020;          % length (m)
phase=pi;          % Mag=pi, Dir=-pi/2
K=(2*pi*n^3*r*GAMMA*L)/(G*wl);
I_out=(.5+.5*cos(K*v + phase));
```

Program E2: SIMULINK program and associated MATLAB function for calculating the magnitude and direction MZI transfer functions. The MATLAB function name is inserted into the appropriate SIMULINK “MATLAB Function” block.

[The page contains extremely faint and illegible text, likely bleed-through from the reverse side of the paper. The text is too light to transcribe accurately.]

APPENDIX F: PHASE COHERENT SIMULINK PROGRAMS FOR MACH-ZEHNDER INTERFEROMETERS (MZIs)

This appendix shows the SIMULINK programs to compare and contrast the MZI phase coherent model (Eqn. 11) with the MZI intensity transfer function (Eqn. 4). This program recreates Figure 13. (*File: MZI_phc.mdl*)

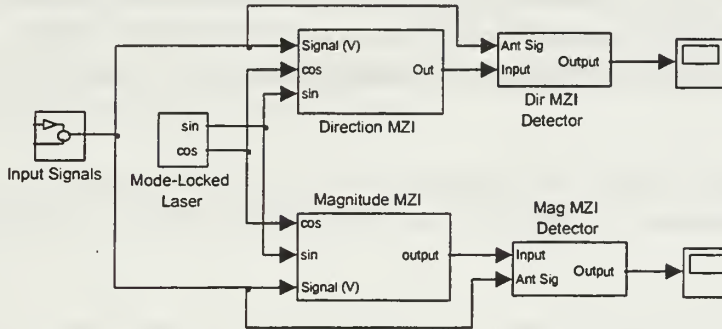


Figure F1: SIMULINK model demonstrating the phase coherent MZI versus the MZI intensity transfer function.

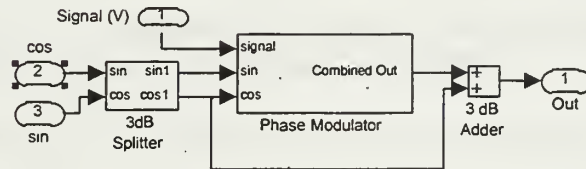


Figure F2: General SIMULINK model of a phase coherent MZI. Used for both directional and magnitude results. This subsystem is part of the MZI subsystems in Figure F1.

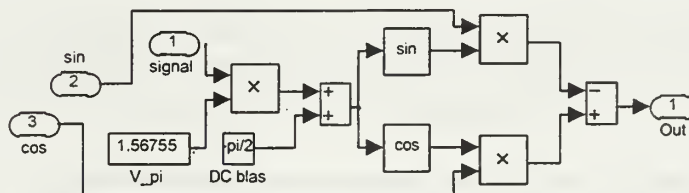


Figure F3: SIMULINK subsystem of the "phase modulator" in Figure F2. Changing the DC bias in this example to π creates the magnitude MZI.

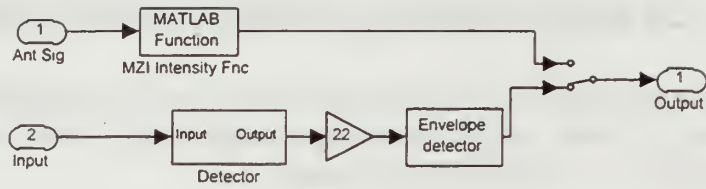


Figure F4: SIMULINK subsystem of phase coherent MZI photodetector and MZI intensity function in the MATLAB function block. Either output can be chosen to go to the scope (Fig. F1) for viewing. This model is used for both the magnitude and direction MZIs.

LIST OF REFERENCES

1. Candy, J.C. and Temes, G.C., "Oversampling Methods for A/D and D/A Conversion," in *Oversampling Delta-Sigma Data Converters*, J.C. Candy and G.C. Temes, Eds., pp 1-29, IEEE Press, New York, NY 1992.
2. Norsworthy, S.R., Schreier, R., and Temes, G.C., *Delta-Sigma Data Converters-Theory, Design, and Simulation*, IEEE Press, 1997.
3. Shoop, B. and Goodman, J., "Optical Oversampled Analog-to-Digital Conversion," *Applied Optics*, Vol. 31, No. 26, 1992.
4. Shoop, B., "Second-Order Cascaded Optical Error Diffusion Modulators for Oversampled Analog-to-Digital Converters," *Optics Communications*, Vol. 102, 1993.
5. Shoop, B. and Goodman, J., "A First-Order Error Diffusion Modulator for Optical Oversampled A/D Conversion," *Optics Communications*, Vol. 97, 1993.
6. Pace, P.E., Ying, S.T., Powers, J.P., and Pieper, R.J., "Integrated Optical Sigma-Delta Modulators," *Optical Eng.*, Vol. 35, No. 7, July 1996.
7. Atherton, A.F., "Integrated Optical Fiber Lattice Accumulators," Master's Thesis, Naval Postgraduate School, Monterey, CA, 1997.
8. Saleh, B.E.A. and Teich, M.C., *Fundamentals of Photonics*, John Wiley & Sons, New York, NY, 1991.
9. Yariv, A. and Yeh, Y., *Optical Waves in Crystals*, John Wiley & Sons, New York, NY, 1984.
10. Moslehi, B., Goodman, J.W., Tur, M., and Shaw, H.J., "Fiber-optic Lattice Signal Processing," *Proc. IEEE*, Vol. 72, No. 7, pp. 909-930, 1984.
11. Jackson, K.P., Newton, S.A., Moslehi, B., Tur, M., Cutler, C.C., Goodman, J.W., and Shaw, H.J., "Optical Fiber Delay Line Signal Processing," *IEEE trans. on Microwave Theory and Techniques*, Vol. MTT-33, No. 3, March 1985.
12. Butler, J.M., "Construction and Measurement of an actively Mode-Locked Sigma Laser," Master's Thesis, Naval Postgraduate School, Monterey, CA, 1998.
13. Pace, P.E., "Introduction to Signals, Signal Conversion, and High Resolution Techniques for Digital Receivers," Class notes, Naval Postgraduate School, Monterey, CA, 20 April 1998.

The first part of the chapter discusses the early years of the United States, from the time of the American Revolution to the end of the 18th century. It covers the political and social changes that shaped the new nation.

The second part of the chapter focuses on the 19th century, a period of rapid growth and expansion. It examines the impact of westward migration, industrialization, and the Civil War.

The third part of the chapter deals with the 20th century, a time of significant social and political transformation. It explores the rise of the Progressive Era, the Great Depression, and the New Deal.

The fourth part of the chapter covers the post-World War II era, characterized by the Cold War, the Civil Rights Movement, and the Vietnam War. It discusses the challenges and achievements of this period.

The fifth part of the chapter looks at the late 20th and early 21st centuries, focusing on the end of the Cold War, the rise of the Internet, and the challenges of globalization.

The sixth part of the chapter discusses the current state of the United States, including the 2008 financial crisis, the Obama administration, and the ongoing political and social debates.

The seventh part of the chapter provides a summary of the key events and trends in the history of the United States, from the founding to the present day.

The eighth part of the chapter offers a perspective on the future of the United States, considering the challenges and opportunities that lie ahead.

The ninth part of the chapter discusses the role of the United States in the world, from its emergence as a global superpower to its current position as a leading nation.

The tenth part of the chapter provides a final reflection on the history of the United States, highlighting the values and ideals that have shaped the nation.

The eleventh part of the chapter offers a concluding thought on the importance of understanding the history of the United States in the context of the world.

The twelfth part of the chapter provides a final summary of the key points discussed in the chapter.

INITIAL DISTRIBUTION LIST

	No. of Copies
1. Defense Technical Information Center 8725 John J. Kingman Rd., STE 0944 Ft. Belvoir, VA 22060-6218	2
2. Dudley Knox Library Naval Postgraduate School 411 Dyer Rd. Monterey, CA 93943-5101	2
3. Chairman, Code EC Department of Electrical and Computer Engineering Naval Postgraduate School Monterey, CA 93943-5121	1
4. Prof. Phillip E. Pace, Code EC/Pc Department of Electrical and Computer Engineering Naval Postgraduate School Monterey, CA 93943-5121	2
5. Prof. John P. Powers, Code EC/Po Department of Electrical and Computer Engineering Naval Postgraduate School Monterey, CA 93943-5121	3
6. Prof. Ronald J. Pieper, Code EC/Pi Department of Electrical and Computer Engineering Naval Postgraduate School Monterey, CA 93943-5121	1
7. Chairman, Code PH Department of Physics Naval Postgraduate School Monterey, CA 93943-5121	1
8. LT Scott Bewley..... 103 James River Rd. Cary, NC 27511	2
9. James Butler 23012 Boaz Dr. Lexington Park, MD 20653	1

12 483NPG 3116
TH
10/99 22527-200 FILE

DUDLEY KNOX LIBRARY



3 2768 00368307 9